JCI The Journal of Clinical Investigation

Interruption of KLF5 acetylation promotes *PTEN*-deficient prostate cancer progression by reprogramming cancer-associated fibroblasts

Baotong Zhang, … , Siyuan Xia, Jin-Tang Dong

J Clin Invest. 2024. https://doi.org/10.1172/JCI175949.

Research In-Press Preview **Oncology**

Graphical abstract

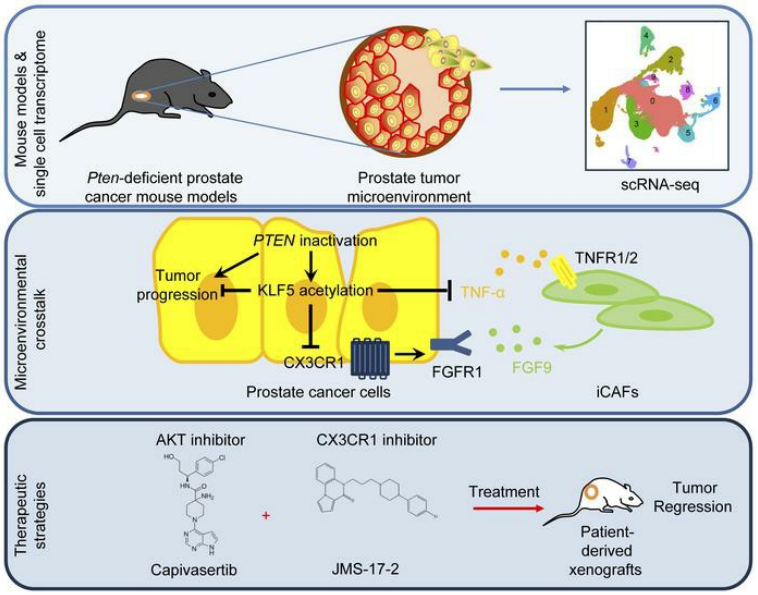

Interruption of KLF5 acetylation promotes *PTEN*-deficient prostate cancer progression by reprogramming cancer-associated fibroblasts

Baotong Zhang[1,2,3,7,*], Mingcheng Liu[1,7], Fengyi Mai[1,7], Xiawei Li[1,4], Wenzhou Wang[1], Qingqing Huang[1], Xiancai Du[1], Weijian Ding[1], Yixiang Li[2,3], Benjamin G. Barwick[2,3], Jianping Jenny Ni[2,3], Adeboye O. Osunkoya[3,5], Yuanli Chen[6], Wei Zhou[2,3], Siyuan Xia[1,2,3], Jin-Tang Dong[1,2,3,*]

[1]Department of Human Cell Biology and Genetics, Southern University of Science and Technology School of Medicine, Shenzhen, Guangdong, China

[2]Department of Hematology and Medical Oncology, Emory University School of Medicine, Atlanta, GA, USA

[3]Winship Cancer Institute, Emory University, Atlanta, GA, USA

[4]Inner Mongolia Institute of Quality and Standardization, Inner Mongolia Administration for Market Regulation, Hohhot, China

[5]Departments of Pathology and Urology, Emory University School of Medicine, Atlanta, GA, USA

[6]Key Laboratory of Major Metabolic Diseases and Nutritional Regulation of Anhui Department of Education, School of Food and Biological Engineering, Hefei University of Technology, Hefei, Anhui, China

[7]These authors contributed equally

*Correspondence: Baotong Zhang (Huiyuan Building 5, Room 303, 1088 Xueyuan Blvd, Nanshan District, Shenzhen, Guangdong, 518055, China, +86075588010102, zhangbt@sustech.edu.cn) and Jin-Tang Dong (Research Building B, Room 508, 1088 Xueyuan Blvd, Nanshan District, Shenzhen, Guangdong, 518055, China, +86075588018032, dongjt@sustech.edu.cn)

Key words: Prostate cancer; Tumor microenvironment; Cancer-associated fibroblasts; Krüppel-like factor 5; Acetylation; PTEN; FGFR1 signaling.

Running title: Ac-KLF5 remodels tumor microenvironment.

Conflict-of-interest statement: The authors declare no conflict of interest.

ABSTRACT

PTEN inactivation is prevalent in human prostate cancer and causes high-grade adenocarcinoma with a long latency. Cancer associated fibroblasts (CAFs) play a pivotal role in tumor progression, but it remains elusive whether and how *PTEN*-deficient prostate cancers reprogram CAFs to overcome the barriers for tumor progression. Herein, we report that *PTEN* deficiency induces KLF5 acetylation; and interruption of KLF5 acetylation orchestrates intricate interactions between cancer cells and CAFs that enhance FGFR1 signaling and promote tumor growth. Deacetylated KLF5 promotes tumor cells to secrete TNF-α, which stimulates inflammatory CAFs to release FGF9. CX3CR1 inhibition blocks FGFR1 activation triggered by FGF9 and sensitizes *PTEN*-deficient prostate cancer to AKT inhibitor capivasertib. This study reveals the role of KLF5 acetylation in reprogramming CAFs and provides a rational for combined therapies using inhibitors of AKT and CX3CR1.

SIGNIFICANCE

PTEN inactivation is a pivotal genetic event in prostate cancer formation, leading to unfavorable clinical outcomes. However, *PTEN* deficiency also causes barriers that constrain tumor progression. Our studies reveal a tumor-suppressive crosstalk between cancer-associated fibroblasts (CAFs) and cancer cells, serving as one of these barriers, with KLF5 acetylation being a pivotal regulator within this dynamic interplay. Interruption of KLF5 acetylation remodels the paracrine crosstalk between cancer cells and inflammatory CAFs by TNF-α and FGF9 signaling, and thus activates FGFR1 signaling to promote cancer progression. CX3CR1 is required by FGF9 to activate FGFR1, and its inhibition sensitizes prostate cancer to AKT inhibitor capivasertib. Our findings unveil the role of KLF5 acetylation in remodeling prostate cancer microenvironment and provide a rationale for combined therapies using inhibitors of AKT and CX3CR1 in patients with *PTEN*-deficient prostate cancer.

HIGHLIGHTS

- Interruption of KLF5 acetylation at K369 promotes the growth of *PTEN*-deficient prostate cancer.
- Interruption of KLF5 acetylation leads to overactivated FGFR1 signaling.
- Cancer cells with deacetylated KLF5 release more TNF-α to signal iCAFs for FGF9 secretion.
- Blocking FGF9/FGFR1 signaling via CX3CR1 inhibition sensitizes cells to AKT inhibitor capivasertib.

INTRODUCTION

Prostate cancer is the most common cancer and the second leading cause of cancer-related death in men in the United States (1). Most prostate cancers are localized and androgen-dependent at diagnosis, and can thus be effectively treated with chemical castration, surgery, and radiation (2). About 12% of prostate cancers progress to metastatic castration-resistant prostate cancer (mCRPC) (3), which contributes to mortality in prostate cancer. Genetic drivers of prostate cancer have been extensively studied and defined for categorizing disease subtypes and developing subtype-specific therapeutic strategies. One of the most potent genetic drivers of prostate cancer is *PTEN*, a tumor suppressor gene mutated in approximately 20% of primary prostate cancers, and in up to 50% of mCRPC (4, 5).

PTEN inactivation results in prostate intraepithelial neoplasia (PIN) by activating PI3K/AKT signaling in genetically engineered mouse models, in which prostate cancer has a long latency to progress to high-grade adenocarcinoma, with metastasis occurring rarely (6-8). The limited tumor progression induced by *PTEN* deficiency suggests additional molecular and cellular responses are activated to constrain tumor progression. In line with the higher frequency of *PTEN* mutations in mCRPC patients, *PTEN* inactivation also co-occurs with other mutations in advanced prostate cancer (9). More directly, loss of *p53* or *Smad4* largely enhances the progression of prostate cancer and contributes to metastatic prostate cancer by overcoming senescence induced by *Pten* deletion (7, 10). Activation of kinase pathways such as RAS/MAPK or HER2 also promote tumor progression of *PTEN*-deficient prostate cancer (11, 12). On the other hand, tumor progression is not a monologue, but an interplay with their surrounding cells in the tumor microenvironment (TME). It remains elusive whether and how TME remodeling is required for *PTEN*-deficient prostate cancer to overcome the progression barriers. Understanding these second hits for the progression of

82 *PTEN*-deficient prostate cancer will provide rationale for combined therapeutic strategies for
83 prostate cancer treatment.

84 TGF-β signaling is prominent in *PTEN*-deficient prostate cancer tumors in addition to PI3K
85 and p53 (10). TGF-β/BMP-SMAD4 signaling is robustly activated in *PTEN*-null prostate cancers
86 (10). Knockout of *Smad4*, a key component of the TGF-β pathway, results in invasive, metastatic,
87 and lethal prostate cancers with 100% penetrance (10). TGF-β is produced by both cancer cells
88 and TME, and reshapes TME actively (13). While TGF-β inhibits tumor growth in early-stage tumor,
89 it induces epithelial-mesenchymal transition (EMT) and promotes cancer metastasis in later-stage
90 tumors (14-19).

91 Acetylation of transcription factor Krüppel-like factor 5 (KLF5) at lysine 369 (K369) has been
92 identified as a posttranscriptional modification downstream of TGF-β. KLF5 acetylation is induced
93 by TGF-β via the SMAD-recruited p300 acetylase (20, 21). Acetylated KLF5 (Ac-KLF5) then forms
94 a transcriptional complex, distinct from that of deacetylated KLF5 (deAc-KLF5), that is essential for
95 TGF-β to function in gene regulation, cell proliferation, and tumorigenesis (20-23). However, it
96 remains unclear whether and how KLF5 acetylation remodels TME in prostate cancer progression.
97 In our most recent study, we found that Ac-Klf5 is essential for proper basal to luminal differentiation
98 in the prostate (24), and loss of Klf5 acetylation in basal progenitor cells results in low-grade PIN
99 (24), suggesting a role of Klf5 acetylation in prostate cancer progression. More importantly, we
100 established a genetically engineered mouse model (GEMM) to conditionally interrupt Klf5
101 acetylation, providing a unique animal model to address the role of Ac-KLF5 in the progression of
102 *PTEN*-deficient prostate cancer (24).

103 Herein, we found that Klf5 acetylation at K358 (a homologous site of human KLF5 K369) is
104 significantly increased by *Pten* loss in mouse prostates and p-AKT activation in human prostates.

Interruption of Klf5 acetylation promotes tumor growth in *Pten*-deficient prostate cancer, as indicated by larger tumor size and enhanced cell proliferation. Mechanistically, the KLF5 acetylation-dependent barrier induced by *PTEN* deficiency constrains prostate tumor growth by attenuating FGFR1 signaling. Deacetylation of KLF5 in prostate cancer cells stimulates inflammatory cancer-associated fibroblasts (iCAFs) through TNF-α to release FGF9, which in turn activates FGFR1 signaling in prostate cancer cells. In addition to the paracrine signaling, deAc-KLF5 induces CX3CR1, which FGF9 requires to activate FGFR1 signaling. Inhibition of CX3CR1 sensitizes *PTEN*-deficient prostate cancer to AKT inhibitor capivasertib. This study not only clarifies the role of KLF5 acetylation in reciprocal communications between prostate cancer cells and iCAFs in *PTEN*-deficient tumors, but also provides a proof of concept for post-translational modifications (PTMs) as essential molecular events induced by *PTEN* inactivation to stall prostate cancer progression.

RESULTS

PTEN deficiency induces KLF5 acetylation in mouse and human prostate tumors

KLF5 acetylation at K369 is induced by TGF-β and has been identified as a crucial PTM downstream of TGF-β in mediating its functions (20, 21). Given the robust activation of TGF-β in *PTEN*-deficient prostate cancer, we tested whether KLF5 acetylation at K369 was affected by PTEN/PI3K/p-AKT signaling. Prostate-specific *Pten* knockout led to adenocarcinoma in mouse prostate (6), and induced Klf5 acetylation at K358 (a homologous site of human KLF5 K369, Figure 1, A and B), as indicated by IHC staining. Knockin of $Klf5^{K358R}$ ($Klf5^{KR}$) mutant in *Pten*-null mouse prostate successfully depleted Klf5 acetylation, validating the induction of Ac-KLF5 by *Pten* knockout (Figure 1, A and B).

PTEN loss activated PI3K/AKT signaling to promote prostate cancer progression. In human prostate cancer samples, we found that Ac-KLF5 was significantly higher when AKT was activated (Figure 1, C and D), consistent with the findings in GEMM. We also evaluated the expression levels of total KLF5 in both GEMM and human prostate cancer specimens but did not observe significant differences in tissues with or without AKT activation (Supplemental Figure 1, A and B).

Interruption of Klf5 acetylation by the K358R mutation promotes *Pten*-null prostate tumor growth

Knockin of $Klf5^{KR}$ mutant successfully interrupted Klf5 acetylation in *Pten*-deficient mouse prostates (Figure 1, A and B), providing an ideal model to test how Klf5 acetylation affects *Pten*-deficient prostate cancer. $Klf5^{KR}$ knockin led to larger tumors in 6-month *Pten*-deficient mouse prostates, as indicated by tumor images and prostate weight (Figure 2, A and B). In addition, the

knockin of one allele of *Klf5*^{KR} appeared to efficiently enlarge tumor sizes in 6 months, although the increase in tumor sizes did not reach significance at 1 to approximately 1.5 years, probably due to the considerable variations among prostate weights (Figure 2B). Further pathological evaluations indicated that *Klf5*^{KR} knockin resulted in more proliferative cells in prostate tumors, as suggested by both mitotic figures and Ki67+ cells (Figure 2, C-E), but not significantly altered the expression patterns of epithelial markers, such as Ar, Ck5 and Ck8 (Supplemental Figure 1C). Mouse prostate cancer cells were used for organoid formation assays (Figure 2, F and G). *Klf5*^{KR} knockin gave rise to more and larger organoids, supporting a role of deAc-KLF5 in promoting prostate tumor growth. One allele of *Klf5*^{KR} knockin appeared insufficient to promote organoid formation (Figure 2, F and G), implying that the extent of Klf5 acetylation may be an essential factor in suppressing tumor growth. Collectively, interruption of Klf5 acetylation at K358 promotes prostatic tumor growth by accelerating cell proliferation.

Deacetylation of KLF5 causes hyperactivated FGFR1 signaling in *PTEN*-deficient tumors

To understand the underlying mechanisms by which deacetylation of Klf5 promotes *Pten*-deficient prostate cancer progression, we performed RNA-seq to identify differentially expressed genes (DEGs) in *Pten*-null mouse prostates with or without *Klf5*^{KR} knockin. Anterior and dorsal prostates were dissected for RNA-seq separately to capture gene expression (Figure 3A and Supplemental Dataset 1, 2). In anterior prostates (AP), *Klf5*^{KR} knockin induced 31 genes and suppressed 162 genes (fold change > 2 and p-value < 0.01). In dorsal prostates (DP), *Klf5*^{KR} knockin induced 107 genes and suppressed 80 genes (fold change > 2 and p-value < 0.01). Functional annotations of differential gene expression by Gene Ontology (GO) analysis revealed the top 20 significant (adjusted p-value < 0.05) biological processes in both AP and DP

(Supplemental Figure 2, A and B). Notably, genes regulating cell-cell adhesion were enriched in both AP and DP (Supplemental Figure 2, A and B). Further investigation of the genes associated with the top enriched biological processes suggests that *Klf5*^{KR} knockin enriched several genes involved in cell-cell communications, specifically some cytokines and cytokine receptors (Supplemental Figure 2C). Given Smad4 is induced by *Pten* knockout and constrains tumor progression (10), we compared the DEGs after *Klf5*^{KR} knockin with those caused by *Smad4* knockout. The genes that are upregulated by *Smad4* knockout were enriched in *Klf5*^{KR} knockin-upregulated genes, and the *Smad4* knockout-downregulated genes were enriched in *Klf5*^{KR} knockin-suppressed genes (Supplemental Figure 2D). These findings suggest Klf5 acetylation as a barrier for *Pten*-null prostate cancer progression, just like Smad4 (10).

Focusing on the gene profiles altered by the interruption of Klf5 acetylation, we further performed geneset enrichment analysis (GSEA) by using a geneset library containing 124 prostate-associated genesets from the Molecular Signatures Database (MSigDB). Interestingly, FGFR1-regulated genesets were among the top enriched sets in both AP and DP (Figure 3B). FGFR1-induced genes were significantly enriched among *Klf5*^{KR} knockin upregulated genes, and FGFR1-downregulated genes were significantly enriched in *Klf5*^{KR} knockin suppressed genes (Figure 3C). The enrichment was significant in both AP and DP (Figure 3C). These GSEA data clearly indicate that interruption of Klf5 acetylation at K358 further enhanced FGFR1 signaling in *Pten*-deficient prostate tumors.

We also confirmed the activation of Fgfr1 signaling in *Pten*-deficient mouse prostates with *Klf5*^{KR} knockin by detecting the phosphorylated Frs2, Erk, and Akt, the canonical downstream signals of Fgfr1 (25). As expected, interruption of Klf5 acetylation at K358 significantly induced the activation of Frs2, Erk, and Akt (Figure 3D), indicating that the acetylation of Klf5 at K358 constrains

Fgfr1 activation in *Pten* knockout mouse prostates. The activation of Fgfr1 by $Klf5^{KR}$ knockin was also confirmed by Western blotting (Supplemental Figure 1D), and consistent results were achieved.

ScRNA-seq reveals an enhanced FGF signaling from fibroblasts to cancer cells

To investigate whether and how a TME signaling is attributed to the FGFR1 overactivation, we performed single-cell RNA sequencing (scRNA-seq) to analyze the crosstalk between prostate cancer cells and other types of cells in the microenvironment. We profiled 61,713 individual cells from fresh dissociated whole prostates of four 16-week-old $PB^{Cre;}Pten^{-/-}$ mice after quality control. These cells include 14,464 and 18,024 cells from two $Klf5^{WT}$ (WT) mice, and 12,310 and 16,915 cells from two $Klf5^{KR}$ (KR) mice. Clustering analysis identified 10 distinct clusters of 820 to 26543 cells each (Figure 4A). Cells from the four mouse prostates were distributed evenly in all 10 clusters and each cluster contained cells from all the four mice (Supplemental Figure 3A).

To annotate the cell clusters, we performed a differential gene expression analysis, through which we successfully identified distinct marker genes for each cluster. (Figure 4B, Supplemental Figure 3B and Supplemental Dataset 3). We took into account that the cells analyzed in our scRNA-seq assay contained various cell components, including normal mouse prostate cells, prostate cancer cells, and other microenvironmental cells. Therefore, we employed marker genes from Guo et al. for the cell type identification of the normal mouse prostates (26), and those from Chan et al. for the cell type identification of mouse prostate cancer tissues (27). The identities of cell clusters were further validated by marker genes in *PanglaoDB* (28). In most clusters, typical cell lineage-specific markers were found on the top of the marker gene list (Supplemental Figure 3B),

and two representative markers were shown in Figure 4B. Canonical luminal cells markers (e.g., *Krt8* and *Krt18*) were shown in cluster 0, 3, and 8 (Supplemental Figure 3C), and these clusters were subsequently distinguished based on their characteristic gene expressions. In comparison to previous studies, the *Abo*+ luminal cluster demonstrated striking similarity to the luminal A cells, which are a cluster of cells identified in normal prostates (26). The *Krt4*+ luminal cells shared marker genes that align with adenocarcinoma cells displaying luminal phenotypes (27). Remarkably, the *Tff3*+ luminal cluster consistently expresses *Tff3*, *Sval1*, *Agr2*, and *Ffar4*, which are the primary marker genes highlighted in *Tff3*+ clusters by Chan et al. (27).

Plotting the cell clusters with Klf5 expression, we found that most of them were the epithelial cells (Figure 4C), consistent with the previous concept that Klf5 is an epithelial factor (29, 30). Notably, the Cre activity of these $PB^{Cre/+}$ mice are specific to the epithelial cells of mouse prostates (31). Considering this specificity, we employed *infercnv* to assess the impact of oncogenic signaling on various epithelial cell types. Interestingly, the *Krt4*+ luminal cells exhibited the highest number of copy number variations (CNVs) (Supplemental Figure 3D), suggesting the presence of cancer-like characteristics of this cell cluster.

We analyzed the cell-cell communications in the TME, revealing that the disruption of Klf5 acetylation in *Pten* deficient tumors resulted in the most substantial changes in interaction strength within *Krt4*+ luminal cells, fibroblasts, and macrophages (Supplemental Figure 3E). Putting the luminal cells as the signaling receiver, fibroblasts were the primary sources of signaling activation subsequent to $Klf5^{KR}$ knockin (Figure 4D). Dissecting the specific signaling pathways, FGF was one of the top signaling pathways that was boosted by deacetylated Klf5 (Supplemental Figure 3F). Strikingly, focusing on the FGF signaling, the *Krt4*+ luminal clusters received the highest FGF signaling after $Klf5^{KR}$ knockin, and the primary source is from fibroblasts (Figure 4E).

Increased FGF9 release in CAFs activates FGFR1 signaling in tumor cells with *Klf5*^{KR} knockin

To further validate the microenvironmental signaling from fibroblasts is attributed to the FGFR1 overactivation, we collected conditioned media (CM) from CAFs derived from *Pten* deficient mouse prostates. We found that these CM were capable of inducing FGFR1 activation in prostate cancer cells, as indicated by the phosphorylation of ERK and FRS2 (Figure 5A). Moreover, the CM from *Klf5*^{KR} knockin mice were more potent than its counterpart (Figure 5A), suggesting that more cytokines that activate FGFR1 signaling could be released by CAFs from *Klf5*^{KR} knockin mice.

In scRNA-seq data, we found that most FGFs were released by fibroblasts, and *Fgf2*, *Fgf7*, *Fgf9*, *Fgf10* and *Fgf18* were the top differential *Fgfs* that were upregulated in the fibroblasts of *Klf5*^{KR} prostates (Supplemental Figure 4A). Further investigation of the expressed Fgfs in RNA-seq data revealed that *Fgf9* was the only Fgf that was significantly induced by *Klf5*^{KR} mutant in *Pten*-deficient mouse prostates (Supplemental Figure 4B). Focusing on the overlapped Fgf, Fgf9, we confirmed the increased expression levels of Fgf9 by IF (Figure 5B) and IHC staining (Figure 5C). Consistent with scRNA-seq data, our IF and IHC staining data confirmed that the Fgf9 signal mainly occurred in CAFs (Figure 5, B and C). We further isolated CAFs from *Pten* deficient mouse prostates and validated the increase in Fgf9 in the CAFs from *Klf5*^{KR} knockin prostates, as indicated by both realtime qPCR and ELISA (Figure 5, D and E).

FGF9 activated FGFR1 signaling in a dose-dependent manner within 15 minutes in prostate cancer DU 145 cells (Supplemental Figure 4, C and D), as indicated by the phosphorylation of ERK and FRS2. This activation was eliminated by FGFR1 inhibitor AZD4547 or by the knockdown of

FGFR1 (Figure 5F and Supplemental Figure 4E). We also tested the activation effects of FGF9 on FGFR1 signaling in prostate cancer cells with or without *KLF5*^{KR} mutant. Interestingly, the FGFR1 signaling in DU 145 cells with *KLF5*^{KR} mutant was more sensitive to FGF9 (Figure 5G), implying an endogenous pathway in the tumor cells could be involved in the activation of FGFR1 signaling. Collectively, FGF9 is a ligand of FGFR1, mainly released by CAFs and activates FGFR1 signaling in prostate cancer. The overactivated FGFR1 signaling in Ac-Klf5 deficient and *Pten*-null prostate cancers is attributed to the increased FGF9 at least partially.

DeAc-KLF5 upregulates TNF-α in cancer cells to increase FGF9 release by CAFs

Because *PB*^{Cre} contains a probasin promoter and only directs Cre-mediated recombination in epithelial cells of the prostate (31), we asked whether the enhanced secretion of Fgf9 in CAFs is attributed to the stimulus from epithelial cells. Coculture of CAFs with prostate cancer PC-3 and DU 145 cells with *KLF5*^{KR} mutant released more Fgf9 than the wildtype control at both the mRNA and protein levels (Figure 6, A and B), indicating that the signal from prostate cancer cells is essential for CAFs to release FGF9.

A thorough literature review revealed several activators and suppressors of FGF9 (Figure 6C). Focusing on the signaling crosstalk from *Krt4*+ luminal cells to fibroblasts, we conducted a more in-depth analysis of the top differential ligands between Klf5^{KR} and Klf5^{WT} group within the scRNA-seq data (Figure 6D). TNF, encoding TNF-α, was emergent as an FGF9 regulator with significant upregulation in Klf5^{KR} group, as indicated by both scRNA-seq and RNA-seq data (Figure 6, D and E). Through the estimation of signaling pathway activities, we verified an augmented activation of TNF in *Krt4*+ luminal clusters within the *Klf5*^{KR} group (Supplemental Figure 5A). More

directly, the *Cellchat* analysis of scRNA-seq data revealed that *Krt4*+ luminal cells, macrophages and neutrophils were the three predominant sources of TNF signaling enhancement due to $Klf5^{KR}$ knockin (Supplemental Figure 5B).

We further detected the expression levels of TNF-α by IHC staining in the prostates of $PB^{Cre};Pten^{-/-};Klf5^{KR/KR}$ and $PB^{Cre};Pten^{-/-};Klf5^{+/+}$ mice and confirmed that $Klf5^{KR}$ knockin significantly induced TNF-α in *Pten* deficient mouse prostate cancer (Figure 6F). Further IF staining assay indicated that the induced expression of TNF-α by $Klf5^{KR}$ knockin occurred in both epithelial cells and CD11b+ macrophages (Supplemental Figure 5C). To determine whether deAc-KLF5 affects TNF-α secretion in cancer cells, we detected the expression levels of TNF-α in prostate cancer DU 145 cells with $KLF5^{WT}$ and $KLF5^{KR}$ in different culture conditions, including cancer cells alone, cancer cells treated by CM of CAFs, and cancer cells cocultured with CAFs (Figure 6G). As indicated by realtime qPCR and ELISA, DU 145 cells with $KLF5^{KR}$ released more TNF-α (Figure 6G). Interestingly, the basal levels of TNF-α were increased when the cancer cells were treated by CM of CAFs or cocultured with CAFs (Figure 6G), suggesting a potential role of the crosstalk between cancer cells and CAFs in the TNF-α secretion.

Functionally, after 24-hour treatment, TNF-α induced Fgf9 expression levels in CAFs (Figure 6H). Furthermore, in the cocultures of CAFs and DU 145 cancer cells, the blockage of TNF-α by the neutralizing antibodies against TNF-α, TNFR1 and TNFR2 effectively eliminated the increase in Fgf9 secretion of CAFs caused by $KLF5^{KR}$ knockin (Figure 6I). These findings indicate that deacetylation of KLF5 in cancer cells signals CAFs to release more FGF9 in a TNF-α dependent manner.

Klf5 deacetylation amplifies the FGF-TNF signaling interplay between iCAF and tumor cells

To further understand how deacetylation of Klf5 in prostate cancer cells reprogram fibroblasts, three subclusters of fibroblasts were revealed by their distinct marker gene expression (Figure 7A and Supplemental Figure 6A). The three fibroblast clusters comprised an iCAF cluster, which expressed canonical markers like *Dpt*, *Gsn*, *Svep1*, *Plpp3*, and *Il6*; a myofibroblastic CAFs (MyCAF) cluster, which exhibited marker genes such as *Col15a1*, *Tpm2*, *Tnc*, and *Cald*; and an unclassified fibroblast cluster (other fibroblasts) (32). It was evident that deacetylated Klf5 mainly intensified the signaling interaction between *Krt4*+ luminal cells and iCAFs, as revealed by *Cellchat* analysis (Figure 7B and Supplemental Figure 6B). Moreover, the Fgf9 induced by $Klf5^{KR}$ knockin occurred in iCAFs, but not in other types of CAFs (Supplemental Figure 6C). As expected, $Klf5^{KR}$ knockin led to an augmentation of FGF and TNF signaling within the cell subsets including fibroblasts and *Krt4*+ luminal cells (Supplemental Figure 6D).

Impressively, a striking effect of Klf5 deacetylation was observed in the substantial reinforcement of FGF signaling, particularly from iCAFs to *Krt4*+ luminal cells (Figure 7C), whereas the most remarkable enhancement in TNF signaling emerged from *Krt4*+ luminal cells directed towards iCAFs (Figure 7D). These findings support that the FGF-TNF signaling crosstalk enhanced by Klf5 deacetylation mainly occurs between fibroblasts and *Krt4*+ luminal cells. Furthermore, trajectory analysis revealed a differentiation pathway from iCAF to MyCAF (Figure 7E). In the $Klf5^{WT}$ group, the secretion of Fgf9 occurred when iCAFs were well differentiated; In contrast, in the $Klf5^{KR}$ group, Fgf9 was expressed from the early stages of iCAF differentiation and persisted throughout the course of differentiation (Figure 7E).

DeAc-KLF5 upregulates CX3CR1 to enhance FGFR1 activation in *PTEN*-deficient cancer cells

In addition to the paracrine crosstalk between cancer cells and CAFs, FGF9 was more potent in activating FGFR1 signaling in prostate cancer cells with $KLF5^{KR}$ mutant (Figure 5G), suggesting that the overactivated FGFR1 signaling caused by $KLF5^{KR}$ knockin could be attributed to additional endogenous molecular mechanisms in cancer cells. Moreover, Klf5 deacetylation activated autocrine signaling prominently in *Krt4*+ luminal cells, as indicated by *Cellchat* analysis of scRNA-seq (Figure 4D and Supplemental Figure 6B). On the one hand, FGF signaling from *Krt4*+ luminal cells to themselves were elevated in $Klf5^{KR}$ mouse prostates (Figure 4E and 7D). On the other hand, we conducted a comprehensive analysis of the distinct ligands that mediate autocrine signaling within *Krt4*+ luminal cells in $Klf5^{KR}$ mouse prostates using *Nichenet*, and then we assessed the efficacy of these ligands in activating FGFR1 signaling by using GSVA, and thus we found 25 ligands activates FGFR1 signaling consistently (Supplemental Figure 7A and Supplemental Dataset 4). Validating these top ligands and their corresponding receptors in RNA-seq data, we found Cx3cr1 was consistently upregulated in the AP and DP of $Klf5^{KR}$ mouse prostates and listed on the top of differential gene list (Supplemental Figure 7, B and C).

The expression level of Cx3cr1 was increased by $Klf5^{KR}$ knockin in *Pten*-deficient prostate cancer, as suggested by RNA-seq (Figure 8A) and confirmed by IHC staining in the prostates of $PB^{Cre};Pten^{-/-};Klf5^{KR/KR}$ and $PB^{Cre};Pten^{-/-};Klf5^{+/+}$ mice (Figure 8B). Consistently, prostate cancer DU 145 cells with $KLF5^{KR}$ also increased their CX3CR1 expression (Figure 8C). Functionally, knockdown of CX3CR1 suppressed the activation of FGFR1 signaling in DU 145 cells with $KLF5^{WT}$ and $KLF5^{KR}$ and attenuated the hyperactivation of FGFR1 signaling in $KLF5^{KR}$ expressing prostate cancer cells (Figure 8D). The organoid assay was further used to evaluate the effects of CX3CR1

inhibitors on prostate cancer progression in vitro. Consistently, *Klf5*^{KR} knockin promoted the organoid formation of *Pten*-deficient prostate cancer cells (Figure 8E and Supplemental Figure 8A), validating the experimental system. Given the potential off-target effects, we chose two different CX3CR1 inhibitors, AZD8797 and JMS-17-2. The addition of AZD8797 and JMS-17-2 selectively suppressed the growth of organoids with deAc-KLF5 (Figure 8E and Supplemental Figure 8A), indicating that induced Cx3cr1 by *Klf5*^{KR} knockin is an essential mechanism by which *Pten*-deficient prostate cancer cells have an advantage in tumor growth.

CX3CR1 inhibition sensitizes *PTEN*-deficient prostate cancer to AKT inhibitor capivasertib

PTEN deficiency is a prevalent molecular event in advanced prostate cancer and promotes cancer progression by activating PI3K/AKT signaling. Therefore, the AKT inhibitor capivasertib is currently under investigation in phase III clinical trials for both mCRPC (NCT05348577) and metastatic hormone-sensitive prostate cancer (NCT04493853). Capivasertib treatment resulted in a decrease in p-Smad2/3 and Ac-Klf5 in the mouse prostates of *Pten* knockout mouse model (Supplemental Figure 8, B and C). Deacetylation of Klf5 upregulates CX3CR1 (Figure 8, A-D), and CX3CR1 served as a central hub for both paracrine signaling and an endogenous pathway that triggers FGFR1 activation (Figure 4-8 and Supplemental Figure 8C). Therefore, it's likely that AKT inhibition by capivasertib reduces KLF5 acetylation, which in turn upregulates CX3CR1 expression and thus leads to an enhanced activation of the oncogenic FGFR1 signaling. We therefore employed a patient derived xenograft (PDX) model with *PTEN*-deficiency to test whether inhibition of CX3CR1 could sensitize prostate cancer cells to capivasertib. The PDX used in this study demonstrated poor responsiveness to capivasertib (Figure 8, F-H and Supplemental Figure 8, D-E), implying the potential activation of an adaptive resistance mechanism. Strikingly, addition of

CX3CR1 inhibitor JMS-17-2 prominently sensitized these PDXs to capivasertib (Figure 8, F-H and Supplemental Figure 8, D-E). This result conclusively underscores a synergistic effect achieved through the combination of CX3CR1 inhibitors and AKT inhibitors in prostate cancer treatment. Further evaluation of Ac-KLF5, p-FRS2 and Ki67 after the treatment of AKT and/or CX3CR1 inhibitors by IHC staining (Figure 8I), we found that a single inhibitor failed to decrease Ki67+ cells significantly. In contrast, inhibitors of AKT and CX3CR1 synergically reduced Ki67+ cells, consistent with the effects on tumor growth (Figure 8, F-H). Moreover, inhibition of AKT signaling by capivasertib resulted in a decrease in Ac-KLF5 and an increase in p-FRS2, validating an adaptive resistance caused by capivasertib. Synergistic inhibition of CX3CR1 successfully dampened FRS2 phosphorylation, rendering the tumors sensitive to capivasertib again (Figure 8I).

Upregulation of FGF9 and CX3CR1 is associated with FGFR1 activation in *Pten*-deficient human prostate cancer

Klf5 acetylation induced by *Pten* deficiency constrains Fgfr1 activation by suppressing Fgf9 and Cx3cr1. We therefore further evaluated whether FGF9 and CX3CR1 are associated with FGFR1 activation in *PTEN* deficient human prostate cancer.

We firstly investigated whether the expression levels of FGF9 and CX3CR1 are associated with FGFR1 activation in TCGA database. To systematically evaluate the activation of FGFR1 signaling, we employ a single sample gene set enrichment assay (ssGSEA) (33, 34) to identify the levels of FGFR1 activation for 499 cancer samples by using three different FGFR1-related REACTOME genesets. Interestingly, both FGF9 and CX3CR1 were positively correlated with the

score of FGFR1 activation (Figure 9A and Supplemental Figure 9), no matter which REACTOME genesets were used for calculating the score in ssGSEA.

Furthermore, in human prostate cancer tissue assays, we detected p-AKT, FGF9, CX3CR1 and p-FRS2 with IHC staining. Activation of AKT provides a sensitive and faithful evaluation of *PTEN* deficiency (6). We further focused on p-AKT+ samples to figure out whether FGF9 is an active ligand of FGFR1 and whether CX3CR1 is required for FGFR1 activation in *PTEN* deficient prostate cancer (Figure 9B and Supplemental Table 1). The canonical substrate of FGFR1 p-FRS2 was used as a marker of FGFR1 activation.

In 28 p-AKT+ samples, although higher CXC3CR1 was associated with higher p-FRS2, the correlation did not reach significance (Figure 9C). Interestingly, when we categorized the samples with FGF9, we found that CX3CR1 was positively correlated with p-FRS2 significantly in FGF9+ samples (Figure 9D). But in FGF9- samples, the association between CX3CR1 and p-FRS2 disappeared (Figure 9E). On the other hand, FGF9 tended to positively correlate with p-FRS2, but it was not significant (Figure 9F). The positive correlation between FGF9 and p-FRS2 reached significance in $CX3CR1^{high}$ prostate cancer samples and disappeared in $CX3CR1^{low}$ samples (Figure 9, G and H). Collectively, FGF9 and CX3CR1 depend on each other to activate FGFR1 in *PTEN*-deficient prostate cancer.

DISCUSSION

Genetic mutations are the driving force of prostate cancer progression, and *PTEN* inactivation is one of the most important genetic events. Up to 70% of primary prostate tumors show loss or alterations in at least one *PTEN* allele (7). Clinically, *PTEN* loss is correlated with unfavorable clinical outcomes, either alone or alongside with other biomarkers, aiding in the differentiation between indolent tumors and aggressive prostate cancer (5). In animal models, single knockout of *Pten* leads to PIN, which can progress to high-grade adenocarcinoma following a long latency, with metastasis occurring rarely (6, 10). This suggests that overcoming barriers caused by *Pten* deficiency is essential for continued progression of prostate cancer. Combined inactivation of *Pten* and *p53* in mouse prostates elicits invasive prostate cancer as early as 2 weeks after puberty and is invariably lethal by 7 months of age (7). *PTEN* inactivation also induces TGF-β/BMP signaling, and knockout of *Smad4* overcomes senescence caused by *Pten* deletion and results in invasive, metastatic and lethal prostate cancers with 100% penetrance (10). Although previous studies documented that p53 and SMAD4 are molecular barriers induced by *PTEN* deficiency, it remains unknown whether PTMs are essential for the progression of *PTEN*-deficient prostate cancer. Our prior findings indicate that KLF5 acetylation at K369 is a crucial event downstream of TGF-β. TGF-β induces KLF5 acetylation in prostate cancer (20, 35), and Ac-KLF5 induced by TGF-β is essential for TGF-β to suppress cell proliferation and tumor growth (20-23). This study further revealed that *Pten* deletion significantly increased Ac-KLF5 expression level in mouse prostate (Figure 1), in line with the robust activation of TGF-β signaling (10). Moreover, interruption of Klf5 acetylation promoted tumor growth, accelerated cell proliferation, enhanced the formation of tumor organoids, and altered Smad4 knockout associated genes in *Pten*-deficient prostate cancer (Figure 2 and Supplemental Figure 2D). Therefore, this study indicates that KLF5 acetylation is a barrier to tumor progression boosted by *PTEN* deficiency and provides evidence for

a PTM as an essential molecular event induced by *PTEN* inactivation to stall prostate cancer progression.

Disturbance of the microenvironmental crosstalk between fibroblasts and epithelial cells is crucial for prostate cancer progression. In our study, interruption of KLF5 acetylation remodels the communications between CAFs and prostate cancer cells, emerging as a pivotal factor enabling *PTEN*-deficient prostate cancer to overcome the progression barriers. FGFs released by fibroblasts act on FGF receptors expressed on the surface of epithelial cells, forming paracrine signaling that is well established and regulates diverse cellular processes of prostate epithelial cells (36, 37). This study deciphers paracrine reciprocal communications between *Pten*-deficient prostate cancer cells and iCAFs coordinated by Ac-KLF5. Interruption of Klf5 acetylation in *Pten*-deficient prostate cancer cells signals iCAFs through TNF-α to promote FGF9 release, which in turn activates FGFR1 signaling in prostate cancer cells (Figure 4-7). Furthermore, deacetylation of Klf5 renders iCAFs to express FGF9 at the early stage of iCAF differentiation (Figure 7E), supporting the role of KLF5 acetylation in iCAF reprogramming. ScRNA-seq analysis indicates that macrophages and neutrophils are additional sources and receivers of TNF signaling, which was amplified by macrophages and neutrophils in $Klf5^{KR}$ mouse prostates (Supplemental Figure 5, A and B). Further IF staining assay revealed that the expression of TNF-α was also induced in both epithelial cells and CD11b+ macrophages (Supplemental Figure 5C). Cx3cr1 was highly expressed in macrophages and has been well recognized for its role in lineage specification and survival of macrophages (38, 39). The expression of *Cx3cr1* was increased in the macrophages of $Klf5^{KR}$ prostates in scRNA-seq data. *Cellchat* revealed that the incoming and outgoing strength of macrophages were enhanced in $Klf5^{KR}$ prostates (Supplemental Figure 3E). Hence, it is conceivable that macrophages might serve as key contributors within the microenvironment that

undergo remodeling due to Klf5 acetylation. CX3CR1 in macrophages has been shown to modulate the secretion of proinflammation cytokines including TNF-α (40), thus it is likely that the increase in TNF-α release in tumor cells is attributed to the higher level of CX3CR1 in $Klf5^{KR}$ prostate cancer cells. It remains elusive how TNF-α stimulates FGF9 secretion in CAFs. NF-κB, a major downstream signaling factor of TNF-α, has potential binding sites for the FGF9 promoter region, as predicted by online-based software OProf. Future studies may examine whether TNF-α stimulates FGF9 release via NF-κB. Targeting this paracrine communication between cancer cells and CAFs would provide an insight into therapeutic strategies for prostate cancer patients.

Mechanistic studies indicate that KLF5 constrains *PTEN*-deficient tumors by attenuating FGFR1 signaling (Figure 3). The activation of FGFR1 signaling in prostate cancer cells (*Krt4*+ luminal cells in scRNA-seq) with KLF5 deacetylation was suggested by GSEA utilizing RNA-seq data from both AP and DP samples (Figure 3C), confirmed by the activation of FRS2, ERK, and AKT, three canonical downstream targets of FGFR1 (25) (Figure 3D), and further addressed by scRNA-seq analysis (Figure 4). In *Pten*-deficient prostate tumors with $Klf5^{KR}$ mutant, overactivation of Fgfr1 signaling was further supported by increased Fgf9 secretion and upregulated Cx3cr1 expression (Figure 5, 8). Notably, FGF9 and CX3CR1 depended on each other to activate FGFR1 in *PTEN*-deficient human prostate cancer (Figure 9). On the other hand, inhibition of AKT by capivasertib reduced Ac-KLF5, which in turn induced FGFR1 activation (Figure 8I and Supplemental Figure 8, B-C), rendering an adaptive mechanism of resistance for AKT inhibitors. In prostate cancer, the expression of FGFR1 is observed in approximately 20% moderately differentiated cases and 40% poorly differentiated cases (41). Induced activation of FGFR1 leads to invasive adenocarcinoma with 100% penetrance after 42-week treatment with chemical inducers of dimerization (42), and knockout of FGFR1 in TRAMP prostate cancer animal models results in

attenuated tumorigenesis (43). In addition, FGFR1 has been identified as one of the three markers to predict indolent prostate cancer (44). Most recently, FGFR1 activation emerges as a crucial factor in regulating phenotypic plasticity during the transition from castration-resistant prostate cancer (CRPC) to neuroendocrine prostate cancer (NEPC), closely associated with metastatic disease (27). Our findings highlight a microenvironmental pathway for FGFR1 activation and provide a rationale for the combined therapy of using AKT and FGFR1 inhibitor in prostate cancer treatment.

Previous studies have suggested oncogenic functions of CX3CR1 in prostate cancer, as the expression of CX3CR1 in prostate cancer epithelial cells directs their circulation to the bone (45, 46) and CX3CL1/CX3CR1 enhances migration and metastasis of prostate cancer cells (47, 48). However, it remains unknown whether and how CX3CR1 impacts FGFR1 signaling. The findings in this study revealed that enhanced expression of Cx3cr1 after *Klf5*^{KR} knockin in *Pten* deficient prostate cancer is an endogenous molecular mechanism by which FGFR1 signaling is activated by its paracrine ligand FGF9 (Figure 8). Knockdown of CX3CR1 or blockage of CX3CR1 by different chemical inhibitors (AZD8797 and JMS-17-2) effectively suppressed FGFR1 activation and the formation of prostate cancer organoids (Figure 8). In human prostate cancer patients, high expression levels of CX3CR1 were required for FGF9 to activate FGFR1 signaling (Figure 9D) and CX3CR1 was positively associated with FGFR1 activation under FGF9 secretion (Figure 9G). These findings disclose a crosstalk between FGFR1 and CX3CR1, although the molecular mechanistic details in this crosstalk remain to be defined. We propose that CX3CR1 could directly phosphorylate FGFR1 upon activation by its ligand CX3CL1. Nevertheless, inhibitors of CX3CR1 effectively sensitized *Pten*-deficient PDX to AKT inhibitor capivasertib (Figure 8, F-H).

Our previous studies identified KLF5 acetylation at K369 as a PTM downstream of TGF-β. TGF-β induces KLF5 acetylation via SMAD-recruited p300 acetylase (20, 21). In this study, *PTEN* deficiency led to KLF5 acetylation at K369 in human and K358 in mouse (Figure 1). Inhibition of Akt activation by capivasertib attenuated p-Smad2/3 and reduced Ac-Klf5 (Supplemental Figure 8C), suggesting a role of the complex of p-Smad2/3 and p300 acetylase in the induction of Klf5 acetylation. Senescence has been defined as a crucial cellular event that constrains tumor progression caused by *PTEN* inactivation (7, 10). It is plausible that KLF5 acetylation causes the senescence induced by *PTEN* loss. Our previous study reported that Ras inhibits TGF-β-induced KLF5 acetylation and transcriptional complex assembly (49). Interestingly, RAS activation aids prostate cancer in overcoming the barriers imposed by *PTEN*-deficiency (11, 50). This corroborates that the removal of KLF5 acetylation is a crucial event in the progression of prostate cancer. In our most recent study, Ac-KLF5 suppressed tumor growth in subcutaneous prostate cancer xenografts but promoted bone metastatic lesions by promoting osteoclast differentiation (35). Consistently, $Klf5^{KR}$ knockin in GEMM further confirms the suppressive function of KLF5 acetylation in primary tumor growth. We did not observe metastasis in bone, liver and lungs of $PB^{Cre};Klf5^{KR/KR};Pten^{-/-}$ mice within 1.5 years, supporting a role of deAc-KLF5 in suppressing tumor motility (35). It's likely that the whole prostate cancer development requires a rapid shift of KLF5 acetylation, which endows prostate cancer cells with plasticity and adaptation to different microenvironments. By this mechanism, deAc-KLF5 accelerates tumor growth in primary tumors and switches to its acetylation form for metastasis.

In summary (Figure 9I), this study defines Klf5 acetylation at K358 as a *PTEN*-deficiency induced PTM, which constrains prostate cancer growth by attenuating FGFR1 activation. Interruption of Klf5 acetylation, on the one hand, signals iCAFs to release FGF9 via TNF-α; on the

other hand, induces CX3CR1 expression in prostate cancer cells. Increased FGF9 and upregulated CX3CR1 cooperate to activate FGFR1 signaling, which leads to the progression of *PTEN*-deficient prostate cancer. *PTEN* deficiency is not only prevalent in prostate cancer, clinical trials using p-AKT inhibitors (e.g., Capivasertib) are also conducted currently combined with abiraterone as a treatment for patients with metastatic prostate cancer. The findings in this study provide clinical rationale for combined therapies using CX3CR1 inhibitor JMS-17-2 and p-AKT inhibitor capivasertib in *PTEN*-deficient prostate cancer.

METHODS

Sex as a biological variable

This study focuses on prostate cancer, which is found only in males. Therefore, all the mice used in this study are male mice. Results in male mice are clinically relevant to human males.

Mouse strains

Klf5^{K358R} knockin mice were established in our previous study (24) and donated to Jackson Laboratory with the name Klf5<LSL-KR> (Stock No. 035317). *PB-Cre4* (*PB*^{Cre}) transgenic mice and *Pten* floxed mice were purchased from NCI Mouse Models of Human Cancers Consortium (MMHCC, Frederick, MD, Cat#: 01XF5) and Jackson Laboratory (Bar Harbor, ME, Cat. No. 004597) respectively. The GEMMs were maintained on a C57BL/6 genetic background. These mice were closely monitored and handled at an Emory University Division of Animal Resources (DAR) facility and the animal facility of Southern University of Science and Technology. The default temperature for housing animals is controllable within a range of 65-86°F and +/- 1°F of the set point year-round and the relative humidity is controlled within a range of 40-50% and within 10% of the set point year-round. By default, animal housing areas are on a 12-hour x 12-hour light/dark cycle.

NSG mice with PDXs were purchased from Jackson Laboratory (Cat# TM00298) via iBio Logistics (Beijing, China). These mice were housing at a DAR facility at Southern University of Science and Technology. Capivasertib and JMS-17-2 were diluted in 10% DMSO, 40% PEG300, 5% Tween-80, and 45% saline for in vivo assay immediately before injection. PDX mice were treated with capivasertib (2.5 mg/kg/day) and/or JMS-17-2 (2.5 mg/kg/day) via intraperitoneal injections.

Cell lines

Prostate cancer PC-3 and DU 145 cell lines were obtained from the American Type Culture Collection (ATCC, Manassas, VA) and propagated according to manufacturer instructions (23).

Tissue microarray

One tissue microarray (# PRC1021) containing 7 normal/benign cases and 95 cancer cases was purchased from PANTOMICS (Fairfield, CA). Some tissue cores were torn or had a dark nonspecific background and had to be excluded from the final statistical analyses. Tissue collection protocol was completed under the approval of the Ethical Committee of each hospital according to the information from PANTOMICS. The pathological features are available in Supplemental Table 2.

Immunofluorescence (IF) and immunohistochemistry (IHC)

Tissue sections were deparaffinized in xylene, rehydrated in graded ethanol, subjected to antigen retrieval by boiling the slides in a pressure cooker for 3 min in a citrate buffer (10 mM trisodium citrate, pH 6.0), permeabilized with 0.5% (vol/vol) Triton X-100. For IHC staining, slides were treated with 3% H_2O_2 for 10 minutes. For both IF and IHC staining, slides were then incubated with 10% goat serum and then with primary antibodies overnight at 4℃. The primary antibodies used for IF and IHC staining included in Supplemental Table 4, in which the Ac-KLF5 antibody was established and reported in our previous study (21, 24, 35).

For IF staining, secondary antibodies Alexa Fluor Dyes (Invitrogen, Carlsbad, CA) were used at 37℃ for 1 hour and DAPI staining was then performed in the dark. Fluorescent images were taken with a Leica SP8 confocal microscope at the Integrated Cellular Imaging Core Facility of Emory University.

For IHC staining, EnVision Polymer-HRP secondary antibodies (Dako, Glostrup, Denmark) were used at room temperature for 1 hour. After the application of DAB-chromogen, tissue sections were stained with hematoxylin, dehydrated, and mounted. IHC staining images were analyzed for counting positive-stained cells and calculating staining intensities by Fiji software.

Western blotting

Briefly, RIPA buffer (Santa Cruz, Dallas, Texas, cat# sc-364162A) was used to collect protein from indicated cells, and then loaded to SDS-PAGE gel (Bio-Rad, Hercules, California) for Western blotting. The general protocol followed the procedures on the website of Cell Signaling Technology. The primary antibodies used in this study included in Supplemental Table 4.

Single cell RNA sequencing (scRNA-seq)

The mouse prostates of 16-week-old *PB^{Cre};Pten$^{-/-}$;Klf5$^{KR/KR}$* (KR) and *PB^{Cre};Pten$^{-/-}$;Klf5$^{+/+}$* (WT) were dissected and minced for scRNA-seq. Two mice per genotype were used. The minced prostate tissue was sent to BerryGenomics (Beijing, China) for single cell preparation, library construction and the following next generation sequencing. Briefly, the single cell suspension was prepared by 5 mg/mL Collagenase Type II digestion and TrypLE dissociation, and then filtered using 40 μm cell strainers. The cells were washed with DPBS (0.04% BSA) for three times and resuscitated to a concentration of 700 ~ 1200 cells/ μL (viability > 85%). ScRNA-seq libraries were prepared using the Chromium Single Cell 3' Reagent Kits v3 (10x Genomics) according to the manufacturer's instructions. For gene expression library construction, 50 ng of amplified cDNA was fragmented and end-repaired, double-size selected with SPRIselect beads, and sequenced on an NovaSeq platform (Illumina) to generate 150 bp paired-end reads.

Isolation of and coculture with cancer associated fibroblasts

After washing with PBS, *Pten*-deficient mouse prostate cancer tissues were dissected, cut and minced into small pieces (1–2 mm^3), digested in 1 mg/mL collagenase I for 30 minutes at 37℃, and seeded into culture flasks with DMEM containing 10% FBS. Fibroblasts grew outwards from the explants and reached 80% confluence after 2 weeks. These CAFs were passaged and cultured for conditioned medium collection and cocultured with prostate cancer DU 145 cells.

Conditioned media were collected from sub-confluent CAFs grown in DMEM with 5% FBS for 72 hours. Prostate cancer DU 145 cells with $KLF5^{WT}$ or $KLF5^{KR}$ were seeded at a density of 5000 cells in 24-well plates with 10000 CAFs. Neutralizing antibodies against human TNF-α (SinoBiology, cat#10602-R10N1), mouse TNFR1 (R&D System, cat#MAB430-100) and TNFR2 (SinoBiology, cat#50128-RN204) were used for blocking TNF-α signaling in the cocultures. After 72 hours, conditioned media were collected from the supernatants of the cocultures for ELISA and the cocultures were collected for RNA isolation. In the cocultures, gene expression levels in mouse CAFs and human prostate cancer cells were detected by realtime qPCR by using species-specific primers.

Statistical analysis

Graphpad Prism (v8.0.1) was used for plotting the data and performing statistical analysis. Readings in all experiments were shown as means ± standard errors. Unpaired Student *t* test was used to determine the statistical significance of differences between two groups and *p*-values of 0.05 or smaller was considered statistically significant. Two-way ANOVA tests were used for the analysis of the differences between the two genotypes. In this scenario, data of each genotype include different images from different animals. Statistical analysis methods are indicated in the figure legends.

Study approval

The experiments using GEMMs were approved by both the Institutional Animal Care and Use Committee (IACUC) of Emory University with an approval number of PROTO201700496 and the IACUC of Southern University of Science and Technology with an approval number of SUSTech-JY202202013. The animal experiments performed using PDXs were approved by the IACUC of Southern University of Science and Technology with an approval number of SUSTech-JY202202013.

The PDXs used in this study were purchased from Jackson Laboratory (Cat# TM00298). For developing JAX PDX resource, Jackson Laboratory established a network of collaborating cancer research centers, which are responsible for any necessary Institutional Review Board (IRB) authorizations and patient consents to allow their tumor tissue to be used in research.

The tissue microarrays were purchased from US Biomax. Each specimen collected from any clinic was consented to by both hospital and individual, and under approval of Ethical Committee of each hospital.

Data availability

The data generated or analyzed during the current study are available within the article, Supplemental information, and attached “Supporting data values”, or from the corresponding authors upon request if any. The source data underlying figures and Supplemental Figures are provided as a “Supporting data values” file. The next generation sequencing data have been deposited in NCBI's Gene Expression Omnibus. The bulk sequencing data (corresponding to Fig. 3, A-C) are accessible through GEO Series accession number GSE253523. The FPKM and fold changes of genes are listed in Supplemental Datasets 1-2. The scRNA-seq data (corresponding to

633 Figures 4 and 7) are accessible through GEO accession number GSE262893. The raw data of
634 scRNA-seq are accessible through BioProject #PRJNA1094424 in Sequence Read Archive (SRA).
635 The significant marker genes in different Seurat clusters are included in Supplemental Dataset 3.

REFERENCES

1. Siegel RL, Miller KD, Wagle NS, and Jemal A. Cancer statistics, 2023. *CA Cancer J Clin.* 2023;73(1):17-48.

2. Body JJ, Casimiro S, and Costa L. Targeting bone metastases in prostate cancer: improving clinical outcome. *Nat Rev Urol.* 2015;12(6):340-56.

3. Kirby M, Hirst C, and Crawford ED. Characterising the castration-resistant prostate cancer population: a systematic review. *Int J Clin Pract.* 2011;65(11):1180-92.

4. Wu RC, Young IC, Chen YF, Chuang ST, Toubaji A, and Wu MY. Identification of the PTEN-ARID4B-PI3K pathway reveals the dependency on ARID4B by PTEN-deficient prostate cancer. *Nat Commun.* 2019;10(1):4332.

5. Jamaspishvili T, Berman DM, Ross AE, Scher HI, De Marzo AM, Squire JA, et al. Clinical implications of PTEN loss in prostate cancer. *Nat Rev Urol.* 2018;15(4):222-34.

6. Wang S, Gao J, Lei Q, Rozengurt N, Pritchard C, Jiao J, et al. Prostate-specific deletion of the murine Pten tumor suppressor gene leads to metastatic prostate cancer. *Cancer cell.* 2003;4(3):209-21.

7. Chen Z, Trotman LC, Shaffer D, Lin HK, Dotan ZA, Niki M, et al. Crucial role of p53-dependent cellular senescence in suppression of Pten-deficient tumorigenesis. *Nature.* 2005;436(7051):725-30.

8. Trotman LC, Niki M, Dotan ZA, Koutcher JA, Di Cristofano A, Xiao A, et al. Pten dose dictates cancer progression in the prostate. *PLoS Biol.* 2003;1(3):E59.

9. Taylor BS, Schultz N, Hieronymus H, Gopalan A, Xiao Y, Carver BS, et al. Integrative genomic profiling of human prostate cancer. *Cancer Cell.* 2010;18(1):11-22.

10. Ding Z, Wu CJ, Chu GC, Xiao Y, Ho D, Zhang J, et al. SMAD4-dependent barrier constrains prostate cancer growth and metastatic progression. *Nature.* 2011;470(7333):269-73.

11. Mulholland DJ, Kobayashi N, Ruscetti M, Zhi A, Tran LM, Huang J, et al. Pten loss and RAS/MAPK activation cooperate to promote EMT and metastasis initiated from prostate cancer stem/progenitor cells. *Cancer Res.* 2012;72(7):1878-89.

12. Ahmad I, Patel R, Singh LB, Nixon C, Seywright M, Barnetson RJ, et al. HER2 overcomes PTEN (loss)-induced senescence to cause aggressive prostate cancer. *Proc Natl Acad Sci U S A.* 2011;108(39):16392-7.

13. Roberts AB, and Sporn MB. Transforming growth factors. *Cancer Surv.* 1985;4(4):683-705.

14. Roberts AB, and Wakefield LM. The two faces of transforming growth factor beta in carcinogenesis. *Proc Natl Acad Sci U S A.* 2003;100(15):8621-3.

15. Massague J. TGFbeta in Cancer. *Cell.* 2008;134(2):215-30.

16. Massague J. TGFbeta signalling in context. *Nat Rev Mol Cell Biol.* 2012;13(10):616-30.

17. Pickup M, Novitskiy S, and Moses HL. The roles of TGFbeta in the tumour microenvironment. *Nat Rev Cancer.* 2013;13(11):788-99.

18. Ikushima H, and Miyazono K. TGFbeta signalling: a complex web in cancer progression. *Nature Reviews Cancer.* 2010;10(6):415-24.

19. Akhurst RJ, and Hata A. Targeting the TGFbeta signalling pathway in disease. *Nat Rev Drug Discov.* 2012;11(10):790-811.

20. Guo P, Zhao KW, Dong XY, Sun X, and Dong JT. Acetylation of KLF5 alters the assembly of p15 transcription factors in transforming growth factor-beta-mediated induction in epithelial cells. *J Biol Chem.* 2009;284(27):18184-93.

21. Guo P, Dong XY, Zhang X, Zhao KW, Sun X, Li Q, et al. Pro-proliferative factor KLF5 becomes anti-proliferative in epithelial homeostasis upon signaling-mediated modification. *J Biol Chem.* 2009;284(10):6071-8.

22. Guo P, Dong XY, Zhao K, Sun X, Li Q, and Dong JT. Opposing effects of KLF5 on the transcription of MYC in epithelial proliferation in the context of transforming growth factor beta. *J Biol Chem.* 2009;284(41):28243-52.

23. Li X, Zhang B, Wu Q, Ci X, Zhao R, Zhang Z, et al. Interruption of KLF5 acetylation converts its function from tumor suppressor to tumor promoter in prostate cancer cells. *International journal of cancer.* 2015;136(3):536-46.

24. Zhang B, Ci X, Tao R, Ni JJ, Xuan X, King JL, et al. Klf5 acetylation regulates luminal differentiation of basal progenitors in prostate development and regeneration. *Nature communications.* 2020;11(1).

25. Wang C, Ke Y, Liu S, Pan S, Liu Z, Zhang H, et al. Ectopic fibroblast growth factor receptor 1 promotes inflammation by promoting nuclear factor-kappaB signaling in prostate cancer cells. *J Biol Chem.* 2018;293(38):14839-49.

26. Guo W, Li L, He J, Liu Z, Han M, Li F, et al. Single-cell transcriptomics identifies a distinct luminal progenitor cell type in distal prostate invagination tips. *Nat Genet.* 2020;52(9):908-18.

27. Chan JM, Zaidi S, Love JR, Zhao JL, Setty M, Wadosky KM, et al. Lineage plasticity in prostate cancer depends on JAK/STAT inflammatory signaling. *Science.* 2022;377(6611):1180-91.

28. Franzen O, Gan LM, and Bjorkegren JLM. PanglaoDB: a web server for exploration of mouse and human single-cell RNA sequencing data. *Database (Oxford).* 2019;2019.

29. Zhang B, Zhang Z, Xia S, Xing C, Ci X, Li X, et al. KLF5 activates microRNA 200 transcription to maintain epithelial characteristics and prevent induced epithelial-mesenchymal transition in epithelial cells. *Molecular and Cellular Biology.* 2013;33(24):4919-35.

30. David CJ, Huang YH, Chen M, Su J, Zou Y, Bardeesy N, et al. TGF-beta Tumor Suppression through a Lethal EMT. *Cell.* 2016;164(5):1015-30.

31. Wu X, Wu J, Huang J, Powell WC, Zhang J, Matusik RJ, et al. Generation of a prostate epithelial cell-specific Cre transgenic mouse model for tissue-specific gene ablation. *Mech Dev.* 2001;101(1-2):61-9.

32. Wang H, Li N, Liu Q, Guo J, Pan Q, Cheng B, et al. Antiandrogen treatment induces stromal cell reprogramming to promote castration resistance in prostate cancer. *Cancer cell.* 2023;41(7):1345-62 e9.

33. Jia Q, Wu W, Wang Y, Alexander PB, Sun C, Gong Z, et al. Local mutational diversity drives intratumoral immune heterogeneity in non-small cell lung cancer. *Nat Commun.* 2018;9(1):5361.

34. Gromeier M, Brown MC, Zhang G, Lin X, Chen Y, Wei Z, et al. Very low mutation burden is a feature of inflamed recurrent glioblastomas responsive to cancer immunotherapy. *Nat Commun.* 2021;12(1):352.

35. Zhang B, Li Y, Wu Q, Xie L, Barwick B, Fu C, et al. Acetylation of KLF5 maintains EMT and tumorigenicity to cause chemoresistant bone metastasis in prostate cancer. *Nature communications.* 2021;12(1):1714.

36. Corn PG, Wang F, McKeehan WL, and Navone N. Targeting fibroblast growth factor pathways in prostate cancer. *Clin Cancer Res.* 2013;19(21):5856-66.

37. Wang C, Liu Z, Ke Y, and Wang F. Intrinsic FGFR2 and Ectopic FGFR1 Signaling in the Prostate and Prostate Cancer. *Front Genet.* 2019;10:12.

38. Zheng J, Yang M, Shao J, Miao Y, Han J, and Du J. Chemokine receptor CX3CR1 contributes to macrophage survival in tumor metastasis. *Mol Cancer.* 2013;12(1):141.

39. Mass E, Ballesteros I, Farlik M, Halbritter F, Gunther P, Crozet L, et al. Specification of tissue-resident macrophages during organogenesis. *Science.* 2016;353(6304).

40. Lee M, Lee Y, Song J, Lee J, and Chang SY. Tissue-specific Role of CX(3)CR1 Expressing Immune Cells and Their Relationships with Human Disease. *Immune Netw.* 2018;18(1):e5.

41. Giri D, Ropiquet F, and Ittmann M. Alterations in expression of basic fibroblast growth factor (FGF) 2 and its receptor FGFR-1 in human prostate cancer. *Clin Cancer Res.* 1999;5(5):1063-71.

42. Acevedo VD, Gangula RD, Freeman KW, Li R, Zhang Y, Wang F, et al. Inducible FGFR-1 activation leads to irreversible prostate adenocarcinoma and an epithelial-to-mesenchymal transition. *Cancer cell.* 2007;12(6):559-71.

43. Yang F, Zhang Y, Ressler SJ, Ittmann MM, Ayala GE, Dang TD, et al. FGFR1 is essential for prostate cancer progression and metastasis. *Cancer Res.* 2013;73(12):3716-24.

44. Irshad S, Bansal M, Castillo-Martin M, Zheng T, Aytes A, Wenske S, et al. A molecular signature predictive of indolent prostate cancer. *Sci Transl Med.* 2013;5(202):202ra122.

45. Jamieson WL, Shimizu S, D'Ambrosio JA, Meucci O, and Fatatis A. CX3CR1 is expressed by prostate epithelial cells and androgens regulate the levels of CX3CL1/fractalkine in the bone marrow: potential role in prostate cancer bone tropism. *Cancer Res.* 2008;68(6):1715-22.

46. Shulby SA, Dolloff NG, Stearns ME, Meucci O, and Fatatis A. CX3CR1-fractalkine expression regulates cellular mechanisms involved in adhesion, migration, and survival of human prostate cancer cells. *Cancer Res.* 2004;64(14):4693-8.

47. Liu P, Liang Y, Jiang L, Wang H, Wang S, and Dong J. CX3CL1/fractalkine enhances prostate cancer spinal metastasis by activating the Src/FAK pathway. *Int J Oncol.* 2018;53(4):1544-56.

48. Xiao LJ, Chen YY, Lin P, Zou HF, Lin F, Zhao LN, et al. Hypoxia increases CX3CR1 expression via HIF-1 and NFkappaB in androgen-independent prostate cancer cells. *Int J Oncol.* 2012;41(5):1827-36.

49. Guo P, Xing C, Fu X, He D, and Dong JT. Ras inhibits TGF-beta-induced KLF5 acetylation and transcriptional complex assembly via regulating SMAD2/3 phosphorylation in epithelial cells. *J Cell Biochem.* 2020;121(3):2197-208.

50. Arriaga JM, Panja S, Alshalalfa M, Zhao J, Zou M, Giacobbe A, et al. A MYC and RAS co-activation signature in localized prostate cancer drives bone metastasis and castration resistance. *Nature Cancer.* 2020.

AUTHOR CONTRIBUTIONS

B.Z. designed and performed most experiments, analyzed the data, wrote and finalized the paper; M.L. and F.M. performed some key animal experiments and some mechanistic studies; S.X., Y.L., W.W., and Q. H. performed some of the animal and cellular experiments; B.Z., X.L. and B.B., performed bioinformatic analysis; X.D., W.D. and J.J.N. performed genotyping; A.O.O. and Y. C. provided pathology consultancy; W.Z. supervised the study; J.T.D. conceived the project, designed and supervised the study, provided overall guidance, and revised and finalized the manuscript. B.Z. and J.D. acquire fundings. For the co-first authors, the authorship order is assigned according to their contributions to this work.

ACKNOWLEDGEMENTS

We thank Dr. Anthea Hammond of Emory University and Dr. Jamie King for editing the manuscript. This work was supported by the grants 82273079 and 82303045 from the National Natural Science Foundation of China, the grant 2021QN02Y875 from Department of Science and Technology of Guangdong Province, the grants JCYJ20220530113609020, JCYJ20200109141229255 and 20200925174802001 from Science, Technology and Innovation Commission of Shenzhen Municipality, the grant 2021A1515110051 from Guangdong Basic and Applied Basic Research Foundation, the grant W81XWH-18-1-0526 from Department of Defense Prostate Cancer Research Program, and grant R01CA171189 from the National Institutes of Health. The research reported in this publication was supported in part by the Integrated Cellular Imaging Core Facility, the Research Pathology Core Laboratory, and the Emory Integrated Genomics Core of Emory University Winship Cancer Institute under NIH/NCI award number P30CA138292.

FIGURES

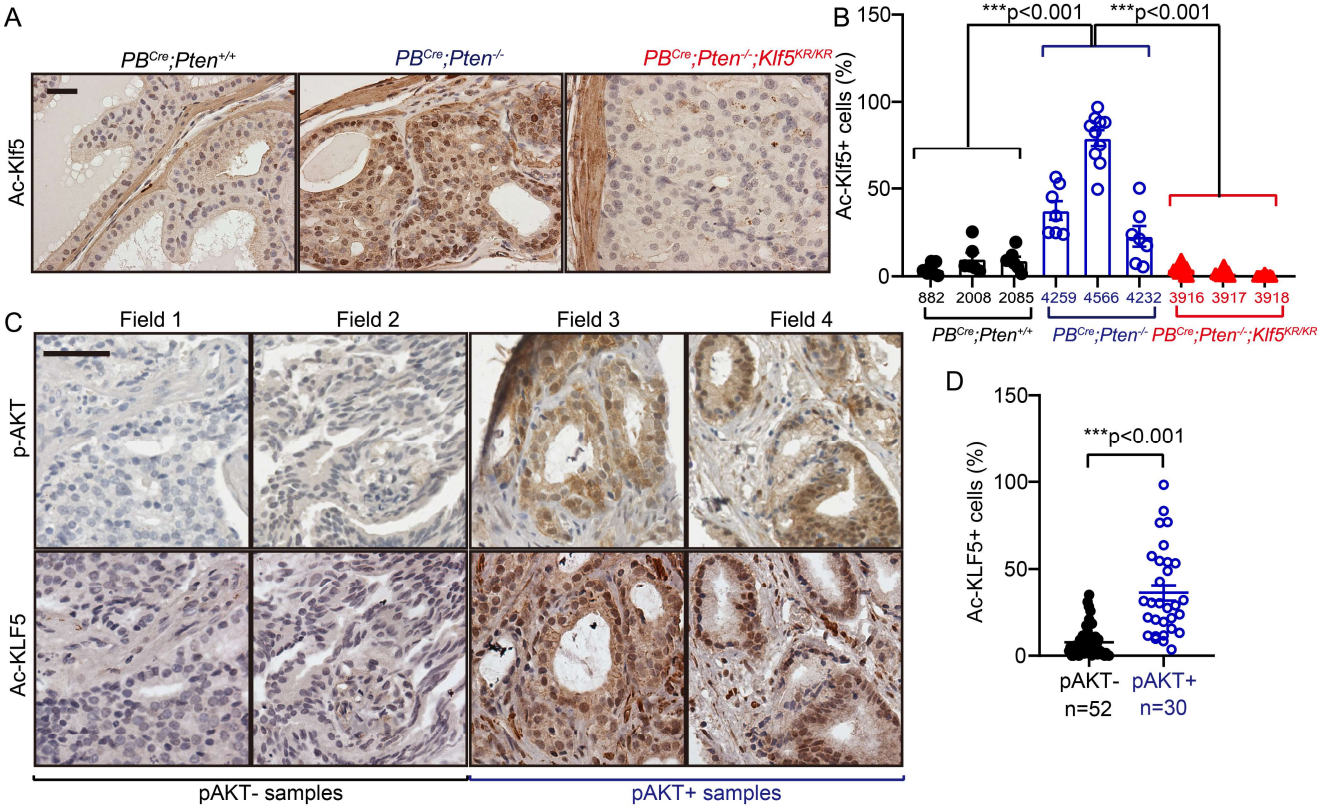

Figure 1. *PTEN* loss induces KLF5 acetylation in mouse and human prostates. (**A**, **B**) IHC staining of acetylated Klf5 at K358 in 4-month-old mice with indicated genotypes, as indicated by representative images (**A**) and statistical analysis (**B**). ***, $p<0.001$ (two-way ANOVA analysis). (**C**, **D**) IHC staining of acetylated KLF5 at K369 in human prostate cancer specimens with or without AKT activation, as indicated by representative images (**C**) and statistical analysis (**D**). ***, $p<0.001$ (two-tailed Student's t-test). Scale bars in **A** and **C**, 50 μm. Data are shown in mean ± S.E.M. Source data are provided as a "Supporting data values" file.

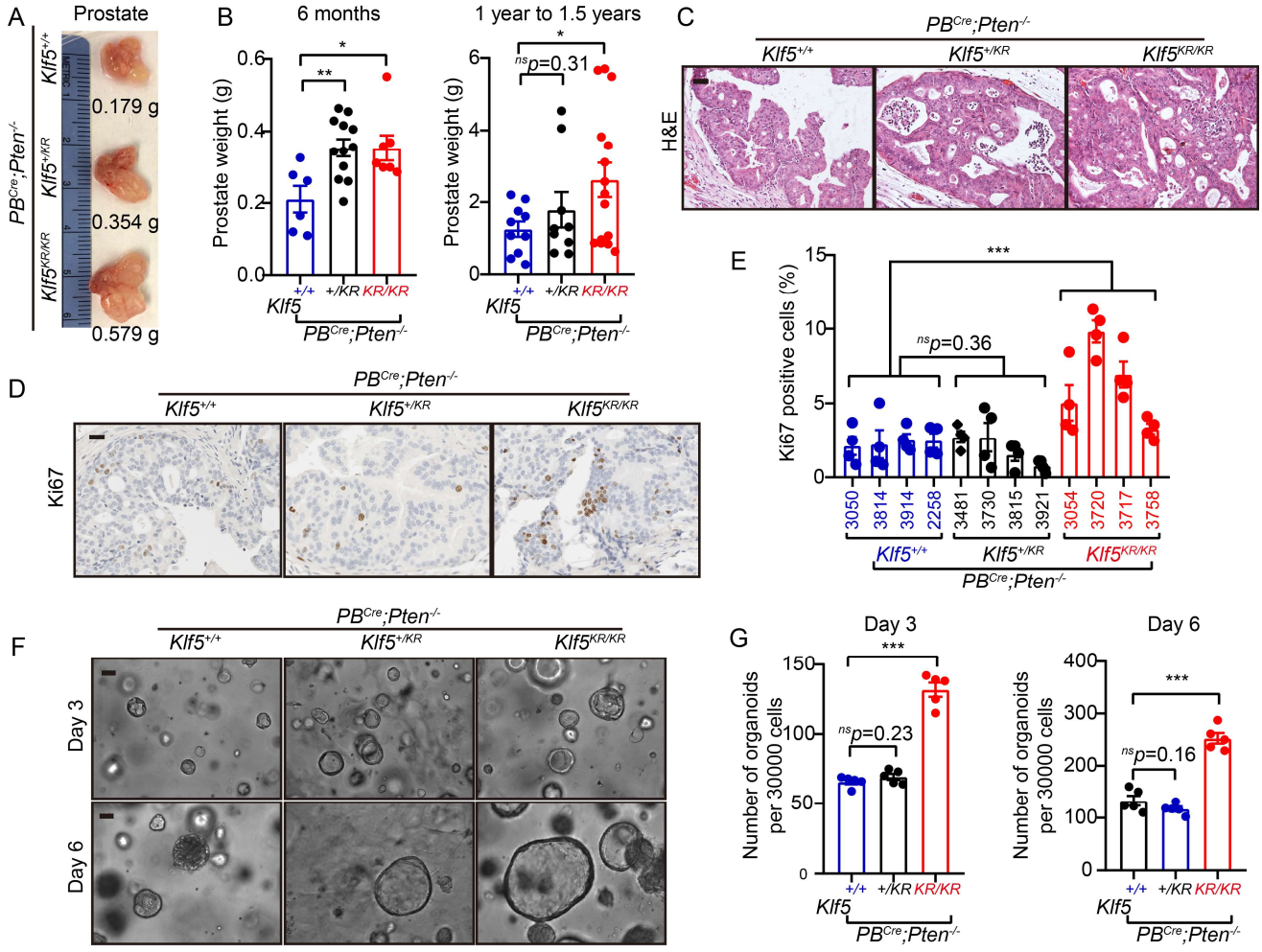

Figure 2. Deacetylation of Klf5 accelerates cell proliferation and the growth of tumors induced by *Pten* loss in the prostate. (**A**, **B**) Knockin of *Klf5*^{K358R} (*Klf5*^{KR}) increased the weight of *Pten*-deficient mouse prostates, as indicated by tumor images (**A**) and tumor weights (**B**). (**C**-**E**) Histological features of 16-week mouse prostates revealed by H&E staining (**C**) and proliferation index detected by Ki67 IHC staining (**D**, **E**). (**F**, **G**) Organoid culture of prostate epithelial cells with indicated genotypes, as indicated by representative organoid pictures (**F**) and statistical analysis of organoid numbers (**G**). Scale bars, 50 μm. Data are shown in mean ± S.E.M. In panels **B** and **G**, two-tailed Student's t-tests were performed. ns, not significant; *, p<0.05; **, p<0.01; ***, p<0.001. In panel **E**, two-way ANOVA analysis was performed. ***, p<0.001. Source data are provided as a "Supporting data values" file.

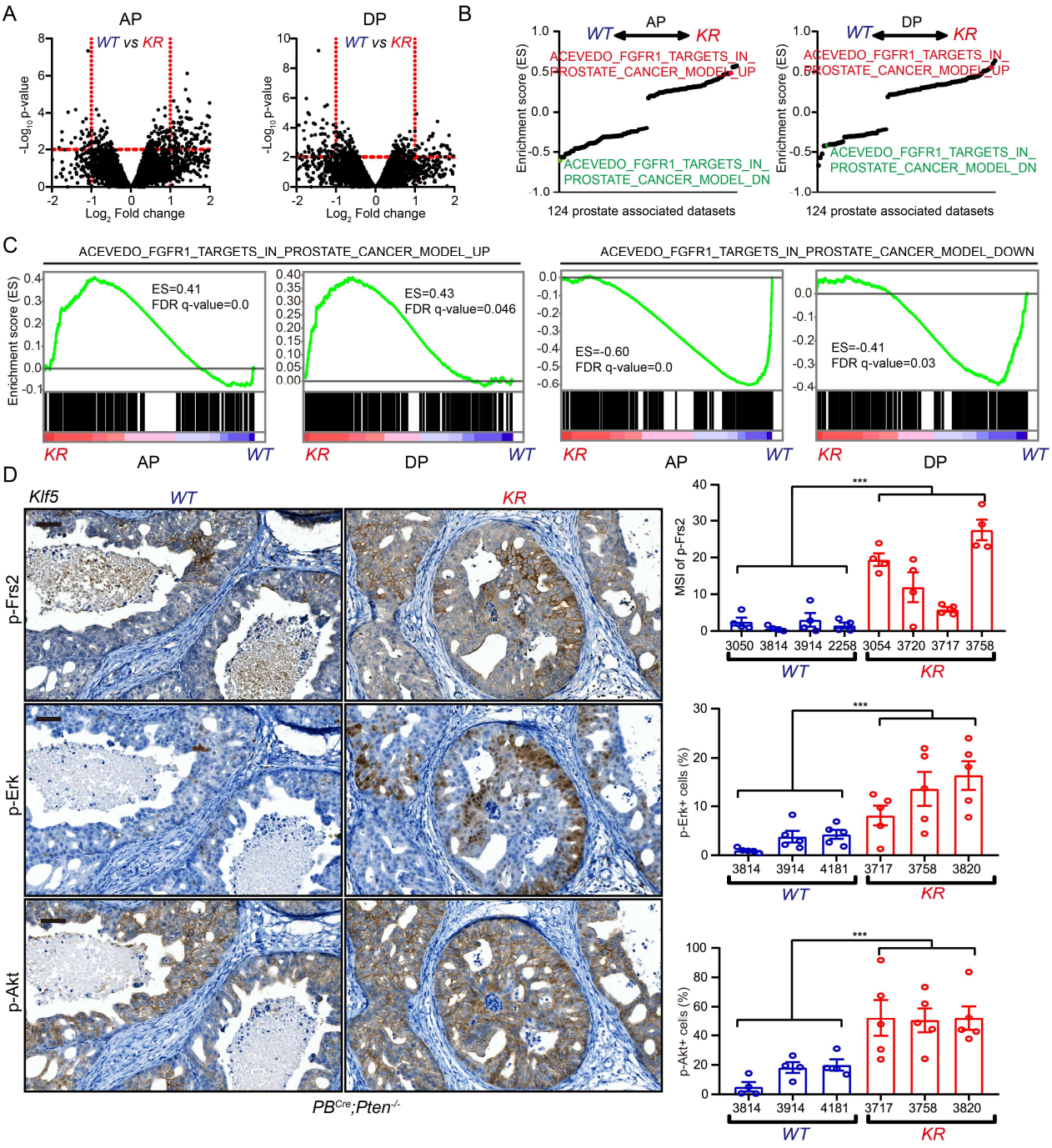

Figure 3. Interruption of Klf5 acetylation enhances FGFR1 signaling in *Pten*-deficient prostate tumors. (**A**) Differential gene expression caused by *Klf5*^{K358R} (*KR*) knockin in *Pten*-loss mouse prostates, as determined by RNA-seq in anterior prostates (AP) and dorsal prostates (DP). (**B**) GSEA of RNA-Seq data of 16-week mice prostates with *PB*^{Cre}*;Pten*$^{-/-}$*;Klf5*$^{KR/KR}$ (KR) and *PB*^{Cre}*;Pten*$^{-/-}$*;Klf5*$^{+/+}$ (WT) in 124 prostate associated datasets. (**C**) GSEA using the genesets containing FGFR1 upregulated and downregulated genes from Acevedo et al., 2007. (**D**) Knockin of *Klf5*^{KR} enhances the activation of Erk, Akt, and Frs2, as detected by IHC staining against p-Erk$^{Thr202/Tyr204}$, p-Akt^{Ser473,} and p-Frs2^{Y436}. Scale bar, 50 μm. MSI, mean staining intensity. Data are shown in mean ± S.E.M. ***, p<0.001 (two-way ANOVA analysis). Source data are provided as a "Supporting data values" file.

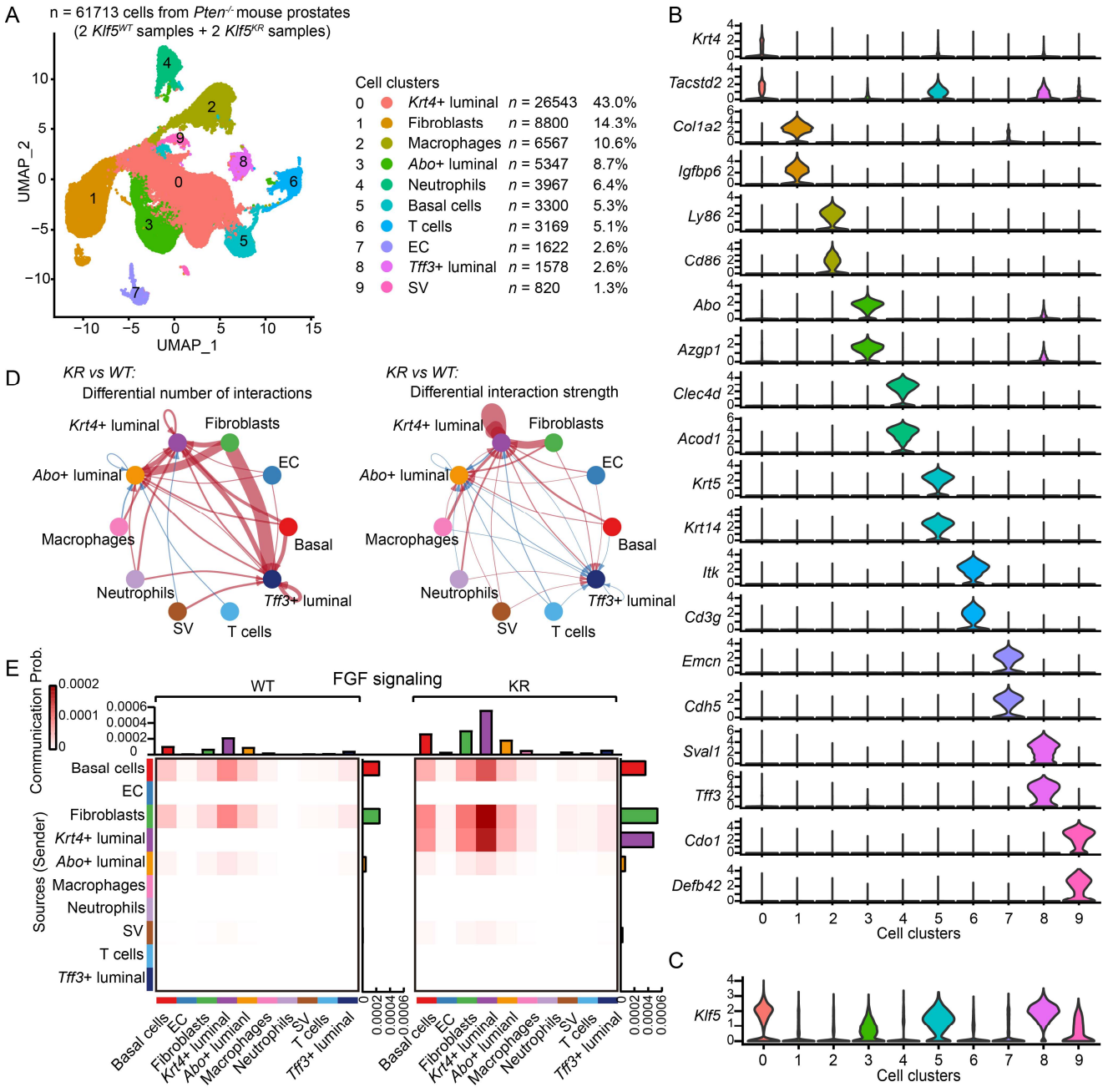

Figure 4. Single-cell transcriptomic analysis reveals an enhanced FGF signaling from fibroblasts to cancer cells after the interruption of Klf5 acetylation. (**A**) Visualization of the annotated clusters of 61713 single cells from *Pten*$^{-/-}$ mouse prostates (n = 2 mice for each genotype) based on the expression of known marker genes by UMAP (left panel). The numbers and percentages of the assigned cell types are summarized in the right panel. EC, endothelial cell; SV, seminal vesicle epithelial cell. (**B, C**) Violin plots showing the expression levels of representative marker genes (**B**) and *Klf5* (**C**) across the main clusters (n = 61713 cells). (**D**) Differential number (left) and strength (right) of interactions from the main clusters to the three luminal clusters between *PB*^{Cre}*;Pten*$^{-/-}$*;Klf5*$^{KR/KR}$ (KR) and *PB*^{Cre}*;Pten*$^{-/-}$*;Klf5*$^{+/+}$ (WT) mouse prostates, as identified by *Cellchat*. The red lines represent activated interactions, while the blue lines represent suppressed interactions in the KR group. Thicker lines indicate greater changes in interactions. (**E**) The communication probability of FGF signaling is calculated by *Cellchat* and shown as a heatmap. Source data are provided as a "Supporting data values" file.

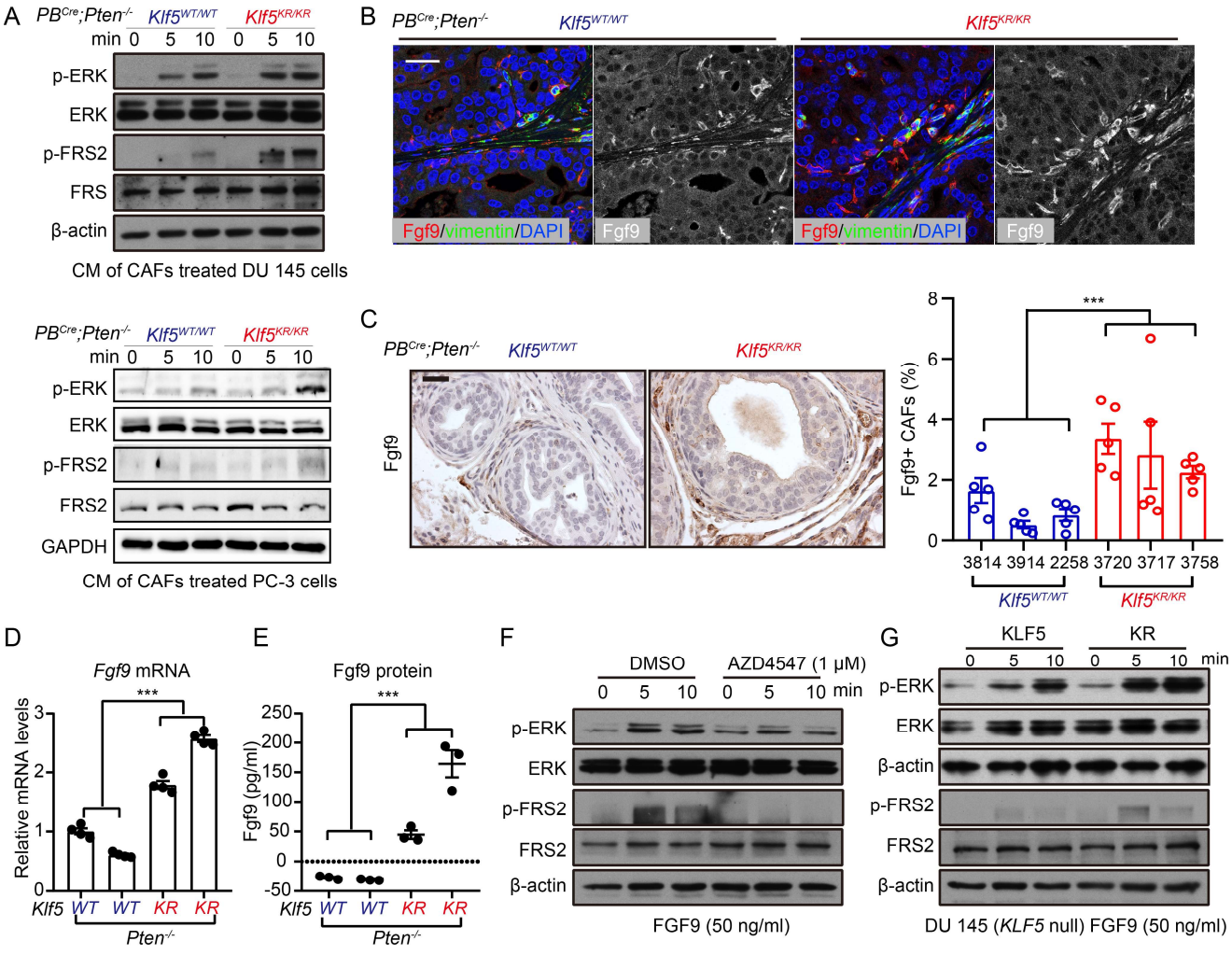

Figure 5. Increased Fgf9 in CAFs contributes to hyperactivated FGFR1 signaling in *Klf5^{KR}* tumor cells with the *Klf5^{KR}* knockin. (**A**) Conditioned media of cancer associated fibroblasts (CAFs) from *PB^{Cre};Pten$^{-/-}$;Klf5$^{KR/KR}$* were more potent to activate FGFR1 in prostate cancer DU 145 and PC-3 cells, as indicated by the expression levels of p-ERK$^{Thr202/Tyr204}$ and p-FRS2^{Y436} detected by Western blotting. (**B**, **C**) Fgf9 expression levels in *Pten*-null mouse prostates with indicated *Klf5* statues, as measured by IF staining (**B**) and IHC staining (**C**). Mice at 16-week were used. Scale bar, 50 μm. (**D**, **E**) Fgf9 expression levels in isolated CAFs from mice with indicated genotypes, as indicated by realtime qPCR (**D**) and ELISA (**E**). WT is *PB^{Cre};Pten$^{-/-}$;Klf5$^{WT/WT}$* and KR is *PB^{Cre};Pten$^{-/-}$;Klf5$^{KR/KR}$*. In panels **C**-**E**, ***, $p<0.001$ (two-way ANOVA analysis). Data are shown in mean ± S.E.M. (**F**) FGF9 induced FGFR1 activation was suppressed by FGFR1 inhibitor AZD4547. (**G**) FGF9 is more potent to activate FGFR1 signaling, as indicated by the expression levels of p-ERK$^{Thr202/Tyr204}$ and p-FRS2^{Y436} by Western blotting. In panels **F** and **G**, DU 145 cells were treated as indicated in the figures. Source data are provided as a "Supporting data values" file.

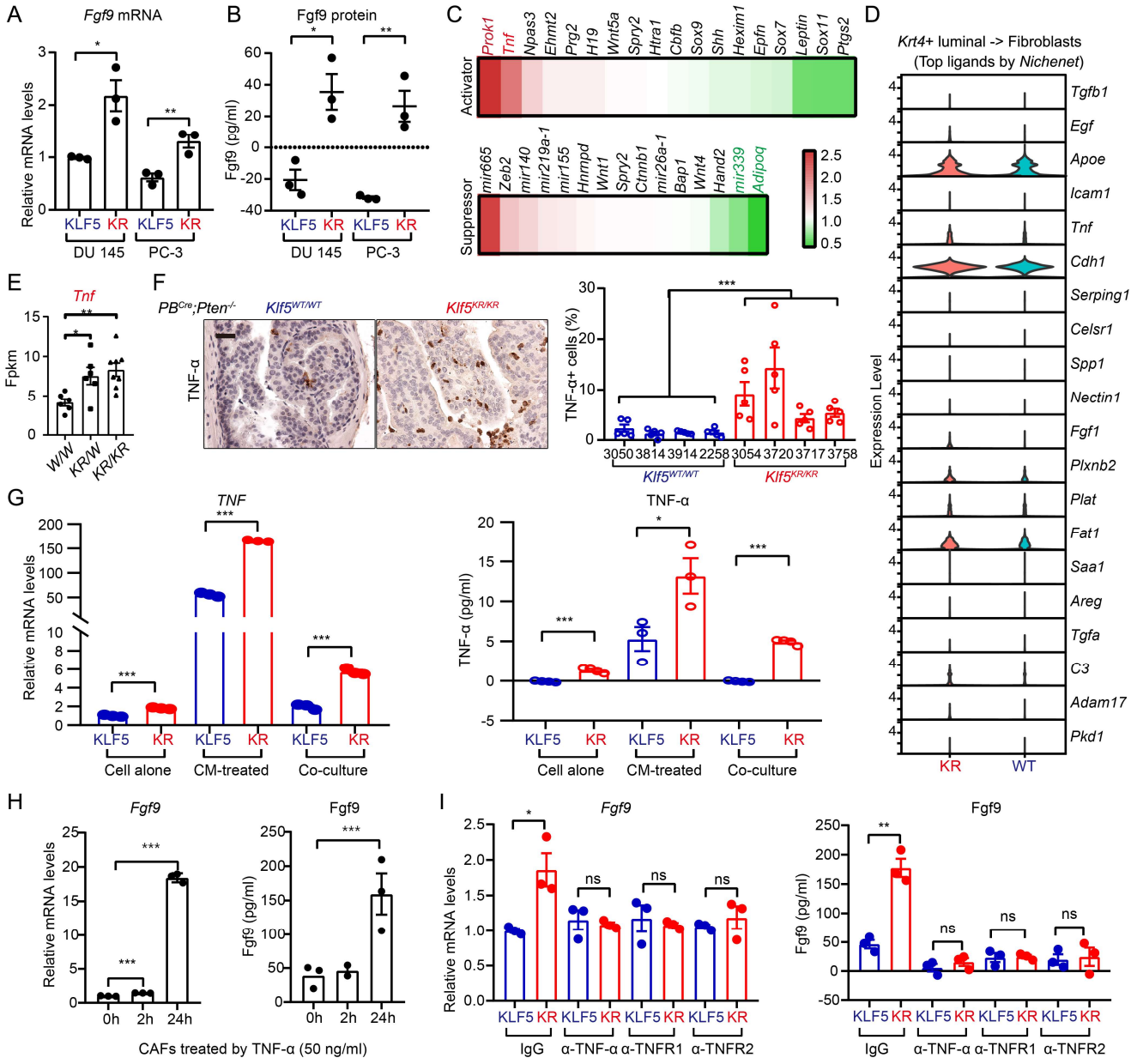

Figure 6. Interruption of Klf5 acetylation upregulates TNF-α in *Pten*-null tumor cells to induce FGF9 secretion in CAFs. (**A**, **B**) Higher Fgf9 expression levels in isolated CAFs when cocultured with two prostate cancer cell lines PC-3 and DU 145 with KLF5^{KR} mutant, as detected by realtime qPCR (**A**) and ELISA (**B**). (**C**) Expression heatmap of activators and suppressors of FGF9 as reviewed from 617 publications. Red and green indicate upregulated and downregulated genes by *Klf5^{KR}* mutant. (**D**) Top ligands that signal fibroblasts from *Krt4*+ luminal are calculated by *NicheNet* and their expression levels in *Krt4*+ luminal cells are shown as violin plots. (**E**) Plots of *Tnf* expression as detected by RNA-seq. *W/W*, *PB^{Cre};Pten$^{-/-}$;Klf5$^{WT/WT}$*; *KR/W*, *PB^{Cre};Pten$^{-/-}$;Klf5$^{WT/KR}$*; *KR/KR*, *PB^{Cre};Pten$^{-/-}$;Klf5$^{KR/KR}$*. (**F**) IHC staining of Tnf-α in mouse prostate tumors with indicated genotypes. Scale bar, 50 μm. (**G**) The expression level of TNF-α is higher in DU 145 cells expressing *KLF5^{KR}* mutant, as indicated by realtime qPCR (left) and ELISA (right). DU 145 cells were cultured as indicated conditions. CAFs from *Pten* deficient mouse prostate tumors were used to produce conditioned media (CM) and coculture with DU 145 cells. (**H**) TNF-α induced Fgf9 expression levels in CAFs, as indicated by realtime qPCR (left) and ELISA (right). (**I**) Blockage of TNF-α signaling by the neutralizing antibodies against TNF-α (5 ng/mL), TNFR1 (20 μg/mL) or

TNFR2 (5 ng/mL) suppressed Fgf9 induction in CAFs by the expression of *KLF5*^{KR} mutant in DU 145 cells. Data are shown in mean ± S.E.M. In panels **A**, **B**, **E** and **G-I**, two-tailed Student's t-tests were performed. ns, not significant; *, p<0.05; **, p<0.01; ***, p<0.001. In panel **F**, two-way ANOVA analysis was performed. ***, *p*<0.001. Source data are provided as a "Supporting data values" file.

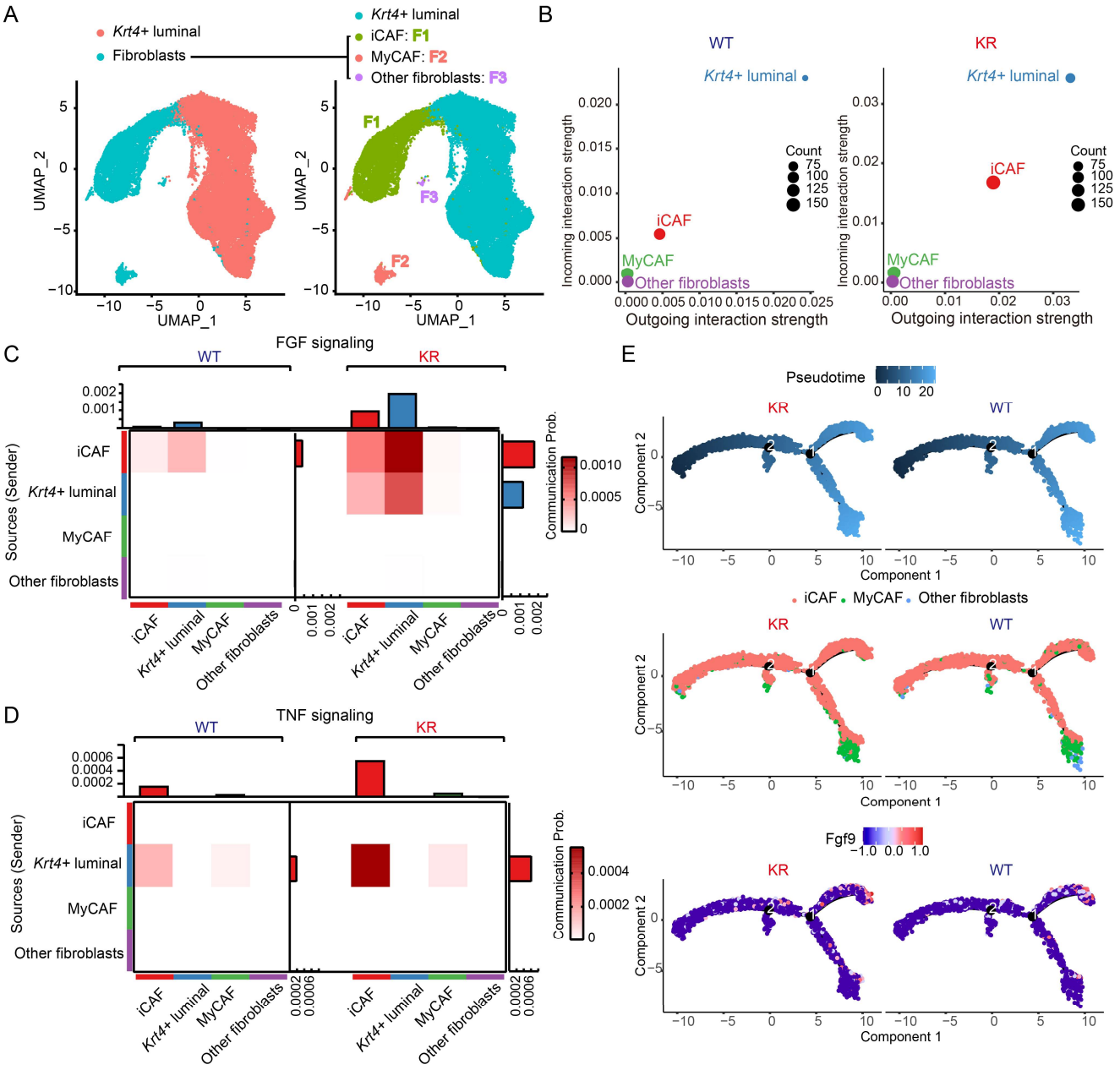

Figure 7. Klf5 deacetylation enhances FGF-TNF signaling crosstalk between iCAF and prostate cancer cells. (**A**) Visualization of the annotated clusters of *Krt4*+ luminal and fibroblasts subsets in scRNA-seq as UMAP (n = 35343 cells). Fibroblasts are further divided into iCAF, MyCAF and undefined fibroblasts (other fibroblasts), based on their representative marker genes. (**B**) Enhanced strength of interactions between iCAF and *Krt4*+ luminal cells are shown after Klf5 deacetylation. (**C**, **D**) The communication probability of FGF (**C**) and TNF (**D**) signaling between *Krt4*+ luminal and different fibroblast subsets is calculated by *Cellchat* and shown as heatmaps. (**E**) CAFs are ordered along pseudotime trajectories by *Monocle2* and celltypes and relative Fgf9 expression levels are shown. Source data are provided as a "Supporting data values" file.

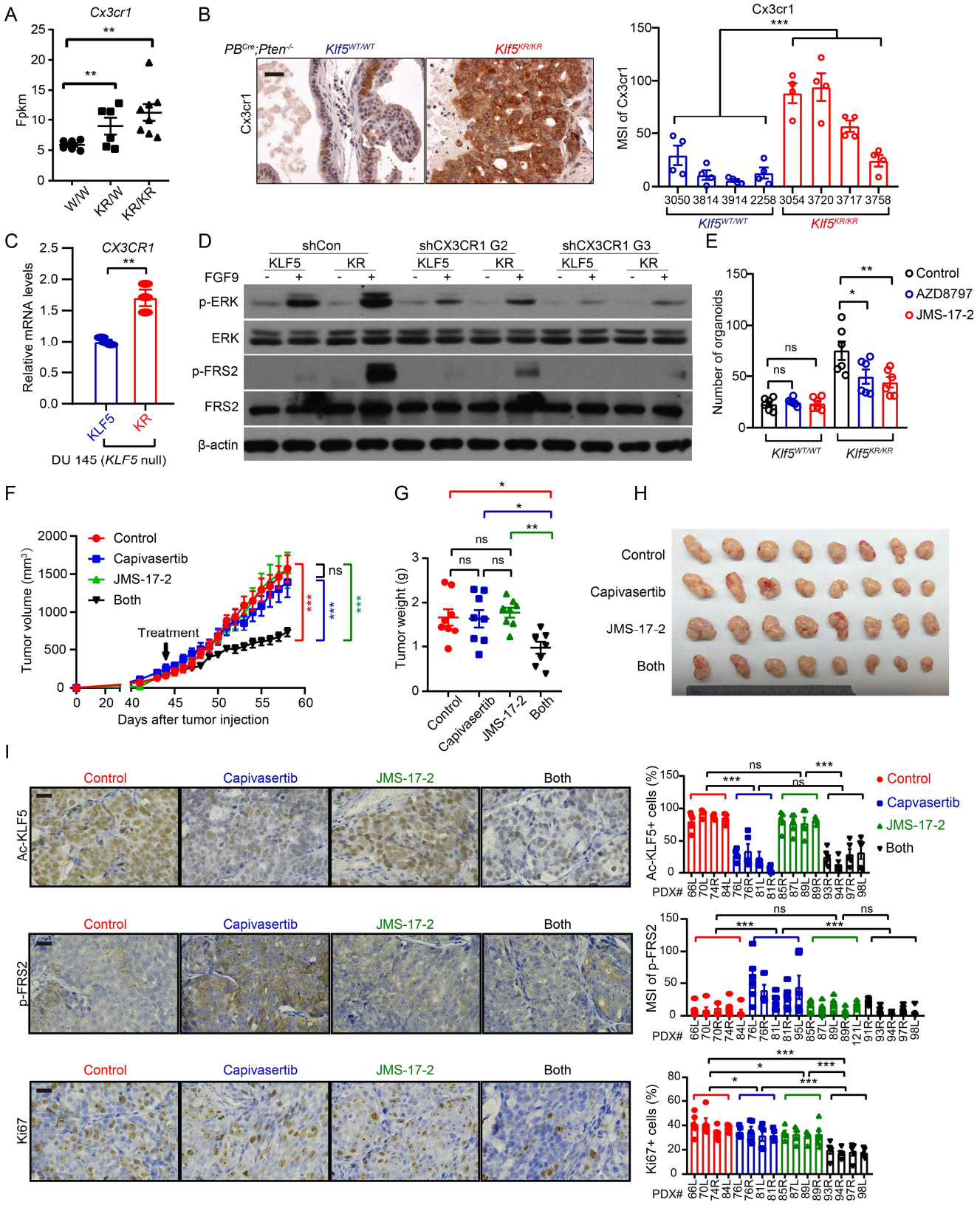

Figure 8. Klf5 deacetylation upregulates CX3CR1 to enhance FGFR1 signaling activity and blocking CX3CR1 sensitizes tumor cells to AKT inhibition. (**A**, **B**) The expression levels of Cx3cr1 were higher in *PB^{Cre};Pten$^{-/-}$;Klf5$^{KR/KR}$* prostate tumors, as indicated by RNA-seq (**A**) and IHC staining (**B**). *W/W*, *PB^{Cre};Pten$^{-/-}$;Klf5$^{WT/WT}$*; *KR/W*, *PB^{Cre};Pten$^{-/-}$;Klf5$^{WT/KR}$*; *KR/KR*, *PB^{Cre};Pten$^{-/-}$;Klf5$^{KR/KR}$*. Scale bar, 50 μm. (**C**) Expression of *CX3CR1* in prostate cancer DU 145 cells with KLF5^{WT} (KLF5) or KLF5^{KR} (KR) by realtime qPCR. (**D**) DU 145 cells expressing KLF5^{WT}

(KLF5) and KLF5^{KR} (KR) were treated with FGF9 (50 ng/mL) for 5 minutes. FGFR1 downstream p-ERK$^{Thr202/Tyr204}$ and p-FRS2^{Y436} were detected by Western blotting. G2 and G3 are two shRNAs of CX3CR1. (**E**) Inhibitors of CX3CR1 selectively suppress the organoid formation of mouse prostate cancer cells with *Klf5^{KR}* mutant in the context of *Pten* deficiency. AZD8797 (50 nM) and JMS-17-2 (1 nM) are two different CX3XR1 inhibitors. (**F**-**H**) *PTEN* deficient PDXs (Jackson lab# TM00298) on NSG mice were treated by AKT inhibitor capivasertib and/or CX3CR1 inhibitor JMS-17-2 as indicated in the figures daily. JMS-17-2 sensitizes capivasertib effects on PDX growth, as indicated by tumor volumes at different times (**F**), tumor weight (**G**) and graphs (**H**) at excision. (**I**) The expression levels of Ac-KLF5, p-FRS2 and Ki67 were evaluated by IHC staining and quantitative analysis. MSI, mean staining intensity. In panels **A**, **C**, **E**, and **G**, two-tailed Student's t-tests were performed. ns, not significant; *, p<0.05; **, p<0.01; ***, p<0.001. In panel **B**, **F** and **I**, two-way ANOVA analyses were performed. ns, not significant; ***, *p*<0.001. Source data are provided as a "Supporting data values" file.

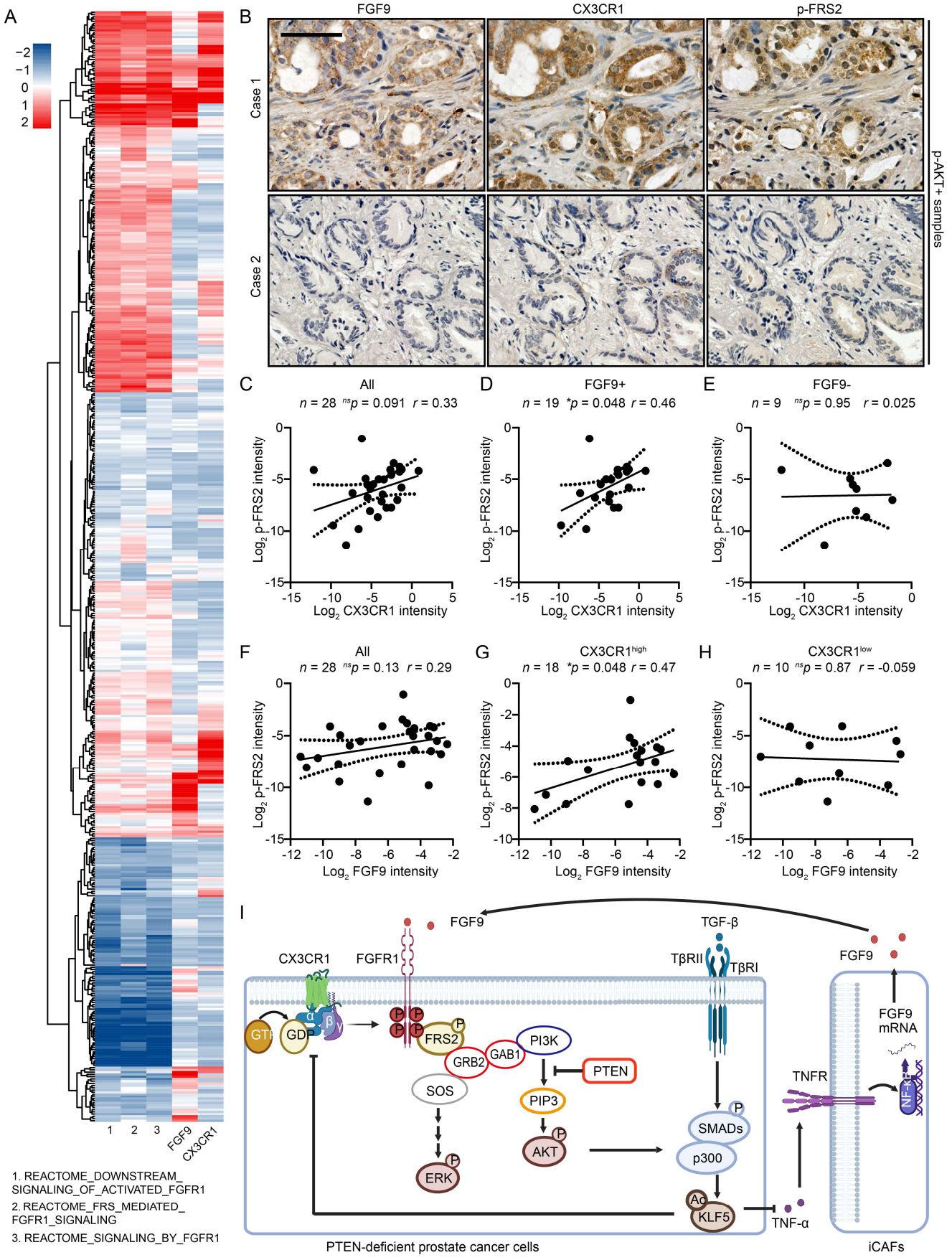

891

892 **Figure 9. Higher expression levels of FGF9 and CX3CR1 correlate with the activation**
893 **of FGFR1 signaling in human prostate cancer.** (**A**) Correlation of FGF9 and CX3CR1 with
894 FGFR1 activation in prostate cancer samples from TCGA database. Single-sample geneset

enrichment assay (ssGSEA) was used to identify the FGFR1 activation for 499 cancer samples by using three different REACTOME genesets. The gene expression levels of FGF9 and CX3CR1 were normalized into a z-score. (**B**) Representative images of IHC staining of FGF9, CX3CR1 and p-FRS2 in p-AKT+ prostate cancer samples. Scale bar, 50 μm. (**C**-**E**) In p-AKT+ tumors, the expression levels of CX3CR1 and p-FRS2 are positively correlated in the condition of FGF9 positive. All, all p-AKT+ tumors (**C**); FGF9+, FGF9+ / p-AKT+ tumors (**D**); FGF9-, FGF9- / p-AKT+ tumors (**E**). (**F**-**H**) In p-AKT+ tumors, the expression levels of FGF9 and p-FRS2 are positively correlated in the condition of $CX3CR1^{high}$. All, all p-AKT+ tumors (**F**); $CX3CR1^{high}$, $CX3CR1^{high}$ / p-AKT+ tumors (**G**); $CX3CR1^{low}$, $CX3CR1^{low}$ / p-AKT+ tumors (**H**). The definition of the expression levels of p-AKT, FGF9, and CX3CR1 refer to Supplemental Table 1. Pearson analyses were performed in panels **C**-**H**. *, $p<0.05$. Source data are provided as a “Supporting data values” file. (**I**) A schematic depicting how *PTEN* deficiency-induced KLF5 acetylation constrains prostate cancer progression by attenuating FGFR1 activation via reprogramming CAFs. This illustrator was generated by *Biorender* with a publication agreement number of *CZ26N14CEQ*.